Late Stage Review

Marco Agnese
PhD student in Applied Mathematics
AMMP Section, Department of Mathematics, Imperial College London
London SW7 2AZ, U.K.
m.agnese13@imperial.ac.uk
Supervisor: Dr. Robert Nürnberg

October 14, 2018

1 Introduction

Fluid flow problems with a moving interface are encountered in many applications in physics, engineering and biophysics. Developing robust and efficient numerical methods for these flows is an important problem and has attracted tremendous interest over the last decade. Apart from the usual difficulties arising from the numerical computation of the fluid flow in the bulk, the accurate approximation of the moving free interface, as well as a suitable description of the conditions that need to hold on the interface, pose serious challenges. Of particular importance is the precise inclusion of surface tension terms, and the correct handling of discontinuity jumps in the material properties and in the pressure at the interface, in order to suppress spurious velocities, which are also called parasitic currents.

This report is extensively based on a paper we submitted some weeks ago, see [2].

We propose a novel finite element approximation for incompressible two-phase Stokes flow that naturally avoids spurious velocities. Our scheme is based on the numerical method introduced in [8], and so uses piecewise linear parametric finite elements to describe the moving discrete interface. In contrast to [8], where the interface and the bulk mesh were totally independent, here we pursue the fitted approach. That means that the interface discretization is always fitted to the bulk mesh, i.e. the discrete interface is made up of edges/faces of elements belonging to the bulk mesh. An advantage of our method is that the discontinuity jumps in the material properties and in the pressure are captured naturally. In particular, we do not need to employ an XFEM-type extension of standard bulk pressure spaces. Surface tension forces are discretized with the help of a variational approximation of curvature that was first proposed in [5, 6]. Combining this was an implicit treatment of the surface tension forces yields an unconditionally stable scheme. Interestingly, the formulation of curvature from [5] leads to a tangential motion of vertices in practice, which guarantees equidistribution in 2d and good meshes in 3d. Overall, our proposed method has the following properties.

- The fully discrete scheme is unconditionally stable in the sense that the total surface energy is monotonically decreasing independent of the chosen time step size.

- In the absence of outer forces, any discrete solution with a stationary interface must have zero velocity globally, i.e. we can prove that there are no stationary solutions with spurious velocities. Similarly, discrete stationary solutions for spherical interfaces are attained for our scheme.
- For the semidiscrete continuous-in-time variant of the fully discrete scheme the volume of the two phases is conserved. The fully discrete scheme itself maintains the enclosed volumes well in practice.
- Thanks to the fitted nature of the finite element method, the pressure jumps at the interface are captured accurately for standard pressure finite element spaces without the need for XFEM extensions.
- The surface tension effects are included with the help of a variational treatment of curvature based on the Laplace-Beltrami operator.
- The surface mesh quality is maintained. In particular, for the semidiscrete scheme an equidistribution property can be shown in 2d.
- The fully discrete scheme uses an implicit approximation of curvature that leads to a coupled linear system of equations to be solved at each time step.

Let us briefly discuss alternative approaches to the numerical approximation of two-phase flow problems. We use a direct description of the interface. In such direct approaches, which are often called front-tracking methods, the interface is either triangulated or presented by a connected set of particles. The discrete interface is advected with the help of the bulk fluid velocities, and quantities on the interface need to be suitably coupled to the bulk equations. In our situation, a finite element parameterization of the unknown interface is employed. We refer e.g. to [39, 4, 38, 19, 20, 8] for further details on front tracking methods, and to [29, 32] for the related immersed boundary method. Another class of approaches is based on interface capturing methods using an indicator function to describe the interface. The volume of fluid (VOF) method and the level set method fall into this category. In the former, the characteristic function of one of the phases is approximated numerically, see e.g. [25, 34, 33]; whereas in the latter, the interface is given as the level set of a function, which has to be determined, see e.g. [37, 36, 31, 23]. Finally, in phase field methods the interface is assumed to have a small, but positive, thickness and an additional parabolic equation, defined in the whole domain, has to be solved in these so-called diffuse interface models. We refer to [26, 3, 30, 17, 28, 1, 24] for details.

2 Mathematical model

2.1 Governing equations

We consider two-phase Stokes flow in a given domain $\Omega \subset \mathbb{R}^d$, where $d = 2$ or $d = 3$. The domain Ω contains two different immiscible, incompressible, viscous fluids (liquid-liquid or liquid-gas) which for all $t \in [0,T]$ occupy time dependent regions $\Omega_+(t)$ and $\Omega_-(t) :=$

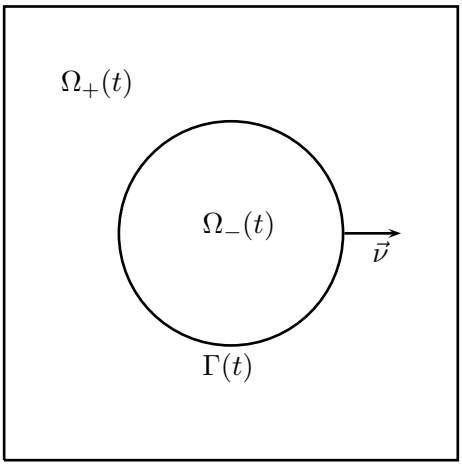

Figure 1: The domain Ω in the case $d = 2$.

$\Omega \setminus \overline{\Omega}_+(t)$ and which are separated by an interface $(\Gamma(t))_{t\in[0,T]}$, $\Gamma(t) \subset \Omega$. See Figure 1 for an illustration. For later use, we assume that $(\Gamma(t))_{t\in[0,T]}$ is a sufficiently smooth evolving hypersurface without boundary that is parameterized by $\vec{x}(\cdot,t) : \Upsilon \to \mathbb{R}^d$, where $\Upsilon \subset \mathbb{R}^d$ is a given reference manifold, i.e. $\Gamma(t) = \vec{x}(\Upsilon, t)$. Then

$$\vec{\mathcal{V}}(\vec{z},t) := \vec{x}_t(\vec{q},t) \qquad \forall\ \vec{z} = \vec{x}(\vec{q},t) \in \Gamma(t) \tag{2.1}$$

defines the velocity of $\Gamma(t)$, and $\vec{\mathcal{V}} \,.\, \vec{\nu}$ is the normal velocity of the evolving hypersurface $\Gamma(t)$, where $\vec{\nu}(t)$ is the unit normal on $\Gamma(t)$ pointing into $\Omega_+(t)$.

Denoting the velocity and pressure by $\vec{u}$ and p, respectively, we introduce the stress tensor

$$\underline{\underline{\sigma}} = \mu\,(\nabla\,\vec{u} + (\nabla\,\vec{u})^T) - p\,\underline{\underline{\mathrm{id}}} = 2\,\mu\,\underline{\underline{D}}(\vec{u}) - p\,\underline{\underline{\mathrm{id}}}\,, \tag{2.2}$$

where $\mu(t) = \mu_+\,\mathcal{X}_{\Omega_+(t)} + \mu_-\,\mathcal{X}_{\Omega_-(t)}$, with $\mu_\pm \in \mathbb{R}_{>0}$, denotes the dynamic viscosities in the two phases, $\underline{\underline{\mathrm{id}}} \in \mathbb{R}^{d\times d}$ is the identity matrix and $\underline{\underline{D}}(\vec{u}) := \frac{1}{2}\,(\nabla\vec{u} + (\nabla\vec{u})^T)$ is the rate-of-deformation tensor.

We consider a two-phase Stokes problem, and so the equations governing the fluid are

$$-\nabla \,.\, \underline{\underline{\sigma}} = \vec{f} \qquad \text{in } \Omega_\pm(t)\,, \tag{2.3a}$$

$$\nabla \,.\, \vec{u} = 0 \qquad \text{in } \Omega_\pm(t)\,, \tag{2.3b}$$

where $\vec{f}$ is a possible forcing term.

On the free surface $\Gamma(t)$, the following conditions need to hold:

$$[\vec{u}]^+_- = \vec{0} \qquad \text{on } \Gamma(t)\,, \tag{2.4a}$$

$$[\underline{\underline{\sigma}}\,\vec{\nu}]^+_- = -\gamma\,\varkappa\,\vec{\nu} \qquad \text{on } \Gamma(t)\,, \tag{2.4b}$$

$$\vec{\mathcal{V}} \,.\, \vec{\nu} = \vec{u} \,.\, \vec{\nu} \qquad \text{on } \Gamma(t)\,, \tag{2.4c}$$

where $\gamma > 0$ is the surface tension coefficient and $\varkappa$ denotes the mean curvature of $\Gamma(t)$, i.e. the sum of the principal curvatures of $\Gamma(t)$, where we have adopted the sign convention that $\varkappa$ is negative where $\Omega_-(t)$ is locally convex. In particular, see e.g. [14], it holds that

$$\Delta_s \vec{\mathrm{id}} = \varkappa\, \vec{\nu} \qquad \text{on } \Gamma(t)\,, \tag{2.5}$$

where $\Delta_s = \nabla_s \,.\, \nabla_s$ is the Laplace-Beltrami operator on $\Gamma(t)$ with $\nabla_s\,.$ and ∇_s denoting surface divergence and surface gradient on $\Gamma(t)$, respectively. Moreover, as usual, $[\vec{u}]^+_- := \vec{u}_+ - \vec{u}_-$ and $[\underline{\underline{\sigma}}\,\vec{\nu}]^+_- := \underline{\underline{\sigma}}_+\,\vec{\nu} - \underline{\underline{\sigma}}_-\,\vec{\nu}$ denote the jumps in velocity and normal stress across the interface $\Gamma(t)$. Here and throughout, we employ the shorthand notation $\vec{g}_\pm := \vec{g}\,|_{\Omega_\pm(t)}$ for a function $\vec{g} : \Omega \times [0,T] \to \mathbb{R}^d$; and similarly for scalar and matrix-valued functions. To close the system we prescribe the initial data $\Gamma(0) = \Gamma_0$ and the boundary condition $\vec{u} = \vec{0}$ on $\partial\Omega$.

Therefore the total system can be rewritten as follows:

$$-2\mu\, \nabla \,.\, \underline{\underline{D}}(\vec{u}) + \nabla\, p = \vec{f} \qquad \text{in } \Omega_\pm(t)\,, \tag{2.6a}$$

$$\nabla \,.\, \vec{u} = 0 \qquad \text{in } \Omega_\pm(t)\,, \tag{2.6b}$$

$$\vec{u} = \vec{0} \qquad \text{on } \partial\Omega\,, \tag{2.6c}$$

$$[\vec{u}]^+_- = \vec{0} \qquad \text{on } \Gamma(t)\,, \tag{2.6d}$$

$$[2\mu\, \underline{\underline{D}}(\vec{u})\,.\,\vec{\nu} - p\,\vec{\nu}]^+_- = -\gamma\,\varkappa\,\vec{\nu} \qquad \text{on } \Gamma(t)\,, \tag{2.6e}$$

$$(\vec{\mathcal{V}} - \vec{u})\,.\,\vec{\nu} = 0 \qquad \text{on } \Gamma(t)\,, \tag{2.6f}$$

$$\Gamma(0) = \Gamma_0\,. \tag{2.6g}$$

2.2 Weak formulation

In order to obtain a weak formulation, we define the function spaces

$$\mathbb{U} := H^1_0(\Omega, \mathbb{R}^d)\,, \qquad \mathbb{P} := L^2(\Omega) \qquad \text{and} \qquad \widehat{\mathbb{P}} := \{\eta \in \mathbb{P} : \int_\Omega \eta \,\mathrm{d}\mathcal{L}^d = 0\}\,,$$

and let $(\cdot,\cdot)$ and $\langle\cdot,\cdot\rangle_{\Gamma(t)}$ denote the L^2–inner products on Ω and $\Gamma(t)$, respectively. In addition, we let $\mathcal{L}^d$ and $\mathcal{H}^{d-1}$ denote the Lebesgue measure in $\mathbb{R}^d$ and the $(d-1)$-dimensional Hausdorff measure, respectively.

Multiplying (2.5) with a test function, and performing integration by parts, yields

$$\langle \varkappa\,\vec{\nu}, \vec{\eta}\rangle_{\Gamma(t)} + \left\langle \nabla_s \vec{\mathrm{id}}, \nabla_s\, \vec{\eta} \right\rangle_{\Gamma(t)} = 0 \quad \forall\ \vec{\eta} \in [H^1(\Gamma(t))]^d\,.$$

Moreover, on noting (2.2) and (2.6e), we have that

$$\begin{aligned}\int_{\Omega_+(t)\cup\Omega_-(t)} (\nabla\,.\,\underline{\underline{\sigma}})\,.\,\vec{\xi}\,\mathrm{d}\mathcal{L}^d &= -\left(\underline{\underline{\sigma}}, \nabla\,\vec{\xi}\right) - \left\langle [\underline{\underline{\sigma}}\,\vec{\nu}]^+_-, \vec{\xi}\right\rangle_{\Gamma(t)} \\ &= \left(p, \nabla\,.\,\vec{\xi}\right) - 2\left(\mu\,\underline{\underline{D}}(\vec{u}), \underline{\underline{D}}(\vec{\xi})\right) + \gamma\left\langle \varkappa\,\vec{\nu}, \vec{\xi}\right\rangle_{\Gamma(t)}\end{aligned}$$

for all $\vec{\xi} \in [H^1_0(\Omega)]^d$. Hence a possible weak formulation of (2.6a–g) is given as follows. Given $\Gamma(0) = \Gamma_0$, for almost all $t \in (0,T)$ find $\Gamma(t)$ and functions $\vec{u} \in \mathbb{U}$, $p \in \widehat{\mathbb{P}}$, $\varkappa \in H^1(\Gamma(t))$ such that

$$2\left(\mu\,\underline{\underline{D}}(\vec{u}),\underline{\underline{D}}(\vec{\xi})\right) - \left(p,\nabla\,.\,\vec{\xi}\right) - \gamma\,\left\langle \varkappa\,\vec{\nu},\vec{\xi}\right\rangle_{\Gamma(t)} = \left(\vec{f},\vec{\xi}\right) \quad \forall\,\vec{\xi} \in \mathbb{U}\,, \tag{2.7a}$$

$$(\nabla\,.\,\vec{u},\varphi) = 0 \quad \forall\,\varphi \in \widehat{\mathbb{P}}\,, \tag{2.7b}$$

$$\left\langle \vec{\mathcal{V}} - \vec{u},\chi\,\vec{\nu}\right\rangle_{\Gamma(t)} = 0 \quad \forall\,\chi \in H^1(\Gamma(t))\,, \tag{2.7c}$$

$$\langle \varkappa\,\vec{\nu},\vec{\eta}\rangle_{\Gamma(t)} + \left\langle \nabla_s\,\vec{\mathrm{id}},\nabla_s\,\vec{\eta}\right\rangle_{\Gamma(t)} = 0 \quad \forall\,\vec{\eta} \in [H^1(\Gamma(t))]^d \tag{2.7d}$$

holds for almost all times $t \in (0,T]$. Here we have observed that if $p \in \mathbb{P}$ is part of a solution to (2.6a–g), then so is $p + c$ for an arbitrary $c \in \mathbb{R}$.

2.3 Energy bound and volume conservation

It is straightforward to show an a priori energy bound and a volume conservation property for the system (2.7a–d). For the former, we recall from e.g. [14, Lemma 2.1] that

$$\frac{\mathrm{d}}{\mathrm{d}t}\,\mathcal{H}^{d-1}(\Gamma(t)) = -\left\langle \varkappa,\vec{\mathcal{V}}\,.\,\vec{\nu}\right\rangle_{\Gamma(t)}\,. \tag{2.8}$$

Hence, on choosing $\vec{\xi} = \vec{u}$ in (2.7a), and noting (2.7b,c), we obtain that

$$\gamma\,\frac{\mathrm{d}}{\mathrm{d}t}\,\mathcal{H}^{d-1}(\Gamma(t)) = -\gamma\,\langle \varkappa\,\vec{\nu},\vec{u}\rangle_{\Gamma(t)} = -2\left(\mu\,\underline{\underline{D}}(\vec{u}),\underline{\underline{D}}(\vec{u})\right) + \left(\vec{f},\vec{u}\right)\,, \tag{2.9}$$

and so in the absence of outer forces, the interfacial energy is monotonically decreasing.

In order to show the volume conservation property, we recall from e.g. [14, Lemma 2.1] that

$$\frac{\mathrm{d}}{\mathrm{d}t}\mathcal{L}^d(\Omega_-(t)) = \left\langle \vec{\mathcal{V}},\vec{\nu}\right\rangle_{\Gamma(t)}\,. \tag{2.10}$$

Hence it follows immediately from the incompressibility condition (2.7b) and (2.7c) that

$$\frac{\mathrm{d}}{\mathrm{d}t}\mathcal{L}^d(\Omega_-(t)) = \langle \vec{u},\vec{\nu}\rangle_{\Gamma(t)} = \int_{\Omega_-(t)} \nabla\,.\,\vec{u}\,\mathrm{d}\mathcal{L}^d = 0\,. \tag{2.11}$$

It will be our aim to introduce a fitted finite element approximation for two–phase Stokes flow that satisfies discrete analogous of (2.9) and (2.11).

3 Numerical method

3.1 Finite element approximation

We consider the partitioning $0 = t_0 < t_1 < \ldots < t_{M-1} < t_M = T$ of $[0,T]$ into possibly variable time steps $\tau_m := t_{m+1} - t_m$, $m = 0,\ldots,M-1$. Moreover, let $\mathcal{T}^m$, $\forall m \geq 0$, be a

regular partitioning of the domain Ω into disjoint open simplices o_j^m, $j = 1, \ldots, J_\Omega^m$. On $\mathcal{T}^m$ we define the finite element spaces

$$S_k^m := \{\chi \in C(\overline{\Omega}) : \chi\,|_{o^m} \in \mathcal{P}_k(o^m)\ \forall\ o^m \in \mathcal{T}^m\} \subset H^1(\Omega), \quad k \in \mathbb{N}\,,$$

where $\mathcal{P}_k(o^m)$ denotes the space of polynomials of degree k on o^m. Moreover, S_0^m is the space of piecewise constant functions on $\mathcal{T}^m$.

Let $\mathbb{U}^m \subset \mathbb{U}$ and $\mathbb{P}^m \subset \mathbb{P}$ be the finite element spaces we use for the approximation of velocity and pressure, and let $\widehat{\mathbb{P}}^m := \mathbb{P}^m \cap \widehat{\mathbb{P}}$. The spaces $(\mathbb{U}^m, \mathbb{P}^m)$ satisfy the LBB inf-sup condition if there exists a constant $C_0 \in \mathbb{R}_{>0}$, independent of $\mathcal{T}^m$, such that

$$\inf_{\varphi \in \widehat{\mathbb{P}}^m} \sup_{\vec{\xi} \in \mathbb{U}^m} \frac{(\varphi, \nabla \,.\, \vec{\xi})}{\|\varphi\|_0\, \|\vec{\xi}\|_1} \geq C_0 > 0\,, \tag{3.1}$$

see [22, p. 114]. Here $\|\cdot\|_0 := (\cdot,\cdot)^{\frac{1}{2}}$ and $\|\cdot\|_1 := \|\cdot\|_0 + \|\nabla\cdot\|_0$ denote the L^2–norm and the H^1–norm on Ω, respectively. We restrict ourselves to the elements P2–P0 and P2–(P1+P0), i.e. we set $\mathbb{U}^m = [S_2^m]^d \cap \mathbb{U}$ and either $\mathbb{P}^m = S_0^m$ or $S_1^m + S_0^m$. Both these elements satisfy the LBB condition (3.1), where we note that the choice P2–(P1+P0) requires the weak constraint that all simplices have a vertex in Ω, see [12].

We consider a fitted finite element approximation for the evolution of the interface $\Gamma(t)$. Let $\Gamma^m \subset \mathbb{R}^d$ be a $(d-1)$-dimensional polyhedral surface approximating the closed surface $\Gamma(t_m)$, $m = 0, \ldots, M$. Let Ω_+^m denote the exterior of Γ^m and let Ω_-^m be the interior of Γ^m. Then $\Omega = \Omega_-^m \cup \Gamma^m \cup \Omega_+^m$, and the fitted nature of our method implies that

$$\overline{\Omega_+^m} = \bigcup_{o \in \mathcal{T}_+^m} \overline{o} \quad \text{and} \quad \overline{\Omega_-^m} = \bigcup_{o \in \mathcal{T}_-^m} \overline{o}\,, \tag{3.2}$$

where $\mathcal{T}^m = \mathcal{T}_+^m \cup \mathcal{T}_-^m$ and $\mathcal{T}_+^m \cap \mathcal{T}_-^m = \emptyset$. Let $\vec{\nu}^m$ denote the piecewise constant unit normal to Γ^m such that $\vec{\nu}^m$ points into Ω_+^m.

In order to define the parametric finite element spaces on Γ^m, we assume that $\Gamma^m = \bigcup_{j=1}^{J_\Gamma} \overline{\sigma_j^m}$, where $\{\sigma_j^m\}_{j=1}^{J_\Gamma}$ is a family of mutually disjoint open $(d-1)$-simplices with vertices $\{\vec{q}_k^m\}_{k=1}^{K_\Gamma}$. Following the notation in [8], see also [6], we define $\underline{V}(\Gamma^m) := \{\vec{\chi} \in [C(\Gamma^m)]^d : \vec{\chi}\,|_{\sigma_j^m} \in \mathcal{P}_1(\sigma_j^m), j = 1, \ldots, J_\Gamma\} =: [W(\Gamma^m)]^d$, where $W(\Gamma^m) \subset H^1(\Gamma^m)$ is the space of scalar continuous piecewise linear functions on Γ^m, with $\{\chi_k^m\}_{k=1}^{K_\Gamma}$ denoting the standard basis of $W(\Gamma^m)$.

Moreover we define $\pi^m : C(\Gamma^m) \to W(\Gamma^m)$ the standard interpolation operator at the nodes $\{\vec{q}_k^m\}_{k=1}^{K_\Gamma}$, and similarly $\vec{\pi}^m : [C(\Gamma^m)]^d \to \underline{V}(\Gamma^m)$. We parameterize the new surface Γ^{m+1} over Γ^m using a parameterization $\vec{X}^{m+1} \in \underline{V}(\Gamma^m)$, so that $\Gamma^{m+1} = \vec{X}^{m+1}(\Gamma^m)$. Before we can state our numerical method, we need to introduce a mass lumped inner product on Γ^m, that is crucial for the desired tangential motion of vertices on Γ^m. This induced tangential motion will lead to good interface mesh properties. If $v, w \in L^\infty(\Gamma^m)$ are piecewise continuous, with possible jumps across the edges of $\{\sigma_j^m\}_{j=1}^{J_\Gamma}$, we define the mass lumped inner product $\langle\cdot,\cdot\rangle_{\Gamma^m}^h$ as

$$\langle v, w\rangle_{\Gamma^m}^h := \tfrac{1}{d} \sum_{j=1}^{J_\Gamma} \mathcal{H}^{d-1}(\sigma_j^m) \sum_{k=1}^{d} (v\,w)((\vec{q}_{j_k}^m)^-), \tag{3.3}$$

where $\{\vec{q}^{\,m}_{j_k}\}_{k=1}^d$ are the vertices of σ^m_j, and where we define the limit $v((\vec{q}^{\,m}_{j_k})^-) := \lim_{\sigma^m_j \ni \vec{p} \to \vec{q}^{\,m}_{j_k}} v(\vec{p})$. We naturally extend (3.3) to vector valued functions. Similarly, we let $\langle \cdot, \cdot \rangle_{\Gamma^m}$ denote the standard L^2–inner product on Γ^m.

Then our finite element approximation, which is based on the variational formulation (2.7a–d), is given as follows. Let Γ^0 be an approximation to $\Gamma(0)$. For $m = 0, \ldots, M-1$, find $\vec{U}^{m+1} \in \mathbb{U}^m$, $P^{m+1} \in \widehat{\mathbb{P}}^m$, $\vec{X}^{m+1} \in \underline{V}(\Gamma^m)$ and $\kappa^{m+1} \in W(\Gamma^m)$ such that

$$2\left(\mu^m\, \underline{\underline{D}}(\vec{U}^{m+1}), \underline{\underline{D}}(\vec{\xi})\right) - \left(P^{m+1}, \nabla \,.\, \vec{\xi}\right) - \gamma \left\langle \kappa^{m+1}\, \vec{\nu}^{\,m}, \vec{\xi} \right\rangle_{\Gamma^m} = \left(\vec{f}^{\,m+1}, \vec{\xi}\right) \qquad \forall\ \vec{\xi} \in \mathbb{U}^m\,, \tag{3.4a}$$

$$\left(\nabla \,.\, \vec{U}^{m+1}, \varphi\right) = 0 \quad \forall\ \varphi \in \widehat{\mathbb{P}}^m\,, \tag{3.4b}$$

$$\left\langle \frac{\vec{X}^{m+1} - \vec{\mathrm{id}}}{\tau_m}, \chi\, \vec{\nu}^{\,m} \right\rangle^h_{\Gamma^m} - \left\langle \vec{U}^{m+1}, \chi\, \vec{\nu}^{\,m} \right\rangle_{\Gamma^m} = 0 \quad \forall\ \chi \in W(\Gamma^m)\,, \tag{3.4c}$$

$$\langle \kappa^{m+1}\, \vec{\nu}^{\,m}, \vec{\eta} \rangle^h_{\Gamma^m} + \left\langle \nabla_s\, \vec{X}^{m+1}, \nabla_s\, \vec{\eta} \right\rangle_{\Gamma^m} = 0 \quad \forall\ \vec{\eta} \in \underline{V}(\Gamma^m) \tag{3.4d}$$

and set $\Gamma^{m+1} = \vec{X}^{m+1}(\Gamma^m)$. Here we have defined $\vec{f}^{\,m+1}(\cdot) := \vec{I}^m_2\, \vec{f}(\cdot, t_{m+1})$, where $\vec{I}^m_2$ is the standard interpolation operator onto $[S^m_2]^d$ and $\mu^m = \mu_+\, \mathcal{X}_{\Omega^m_+} + \mu_-\, \mathcal{X}_{\Omega^m_-} \in S^m_0$. We observe that (3.4a–d) is a linear scheme in that it leads to a coupled linear system of equations for the unknowns $(\vec{U}^{m+1}, P^{m+1}, \vec{X}^{m+1}, \kappa^{m+1})$ at each time level. We also note that the scheme (3.4a–d), in the context of an unfitted finite element approximation, has been considered in [8].

3.2 Existence and uniqueness of a discrete solution

Theorem 1. *Let $m \in \{0, \ldots, M-1\}$ and let $(\mathbb{U}^m, \mathbb{P}^m)$ satisfy the LBB condition (3.1). Then there exists a unique solution $(\vec{U}^{m+1}, P^{m+1}, \vec{X}^{m+1}, \kappa^{m+1}) \in \mathbb{U}^m \times \widehat{\mathbb{P}}^m \times \underline{V}(\Gamma^m) \times W(\Gamma^m)$ to (3.4a–d).*

Proof. As the system (3.4a–d) is linear, existence follows from uniqueness. In order to establish the latter, we consider the system: Find $(\vec{U}, P, \vec{X}, \kappa) \in \mathbb{U}^m \times \widehat{\mathbb{P}}^m \times \underline{V}(\Gamma^m) \times W(\Gamma^m)$ such that

$$2\left(\mu^m\, \underline{\underline{D}}(\vec{U}), \underline{\underline{D}}(\vec{\xi})\right) - \left(P, \nabla \,.\, \vec{\xi}\right) - \gamma \left\langle \kappa\, \vec{\nu}^{\,m}, \vec{\xi} \right\rangle_{\Gamma^m} = 0 \quad \forall\ \vec{\xi} \in \mathbb{U}^m\,, \tag{3.5a}$$

$$\left(\nabla \,.\, \vec{U}, \varphi\right) = 0 \quad \forall\ \varphi \in \widehat{\mathbb{P}}^m\,, \tag{3.5b}$$

$$\left\langle \vec{X}, \chi\, \vec{\nu}^{\,m} \right\rangle^h_{\Gamma^m} - \tau_m \left\langle \vec{U}, \chi\, \vec{\nu}^{\,m} \right\rangle_{\Gamma^m} = 0 \quad \forall\ \chi \in W(\Gamma^m)\,, \tag{3.5c}$$

$$\langle \kappa\, \vec{\nu}^{\,m}, \vec{\eta} \rangle^h_{\Gamma^m} + \left\langle \nabla_s\, \vec{X}, \nabla_s\, \vec{\eta} \right\rangle_{\Gamma^m} = 0 \quad \forall\ \vec{\eta} \in \underline{V}(\Gamma^m)\,. \tag{3.5d}$$

Choosing $\vec{\xi} = \vec{U}$ in (3.5a), $\varphi = P$ in (3.5b), $\chi = \gamma\, \kappa$ in (3.5c) and $\vec{\eta} = \gamma\, \vec{X}$ in (3.5d) yields that

$$2\,\tau_m \left(\mu^m\, \underline{\underline{D}}(\vec{U}), \underline{\underline{D}}(\vec{U})\right) + \gamma \left\langle \nabla_s\, \vec{X}, \nabla_s\, \vec{X} \right\rangle_{\Gamma^m} = 0\,. \tag{3.6}$$

It immediately follows from (3.6) and a Korn's inequality that $\vec{U} = \vec{0}$. In addition, it holds that $\vec{X}$ is equal to a constant on Γ^m, which satisfies, on recalling (3.5c) and $\vec{U} = \vec{0}$, that

$$\left\langle \vec{X}, \chi\, \vec{\nu}^m \right\rangle^h_{\Gamma^m} = 0 \quad \forall\ \chi \in W(\Gamma^m)\,. \tag{3.7}$$

It was shown in [6, Proof of Theorem 2.1] that if Γ^m has no self-intersections, then (3.7) immediately yields that $\vec{X} = \vec{0}$. Since $\Gamma^m = \partial\Omega^m_-$ is the boundary of an open domain, it cannot self-intersect, and hence we obtain that $\vec{X} = \vec{0}$. This means that (3.5d) reduces to

$$\langle \kappa\, \vec{\nu}^m, \vec{\eta} \rangle^h_{\Gamma^m} = 0 \quad \forall\ \vec{\eta} \in \underline{V}(\Gamma^m)\,. \tag{3.8}$$

Let $\vec{\omega}^m \in \underline{V}(\Gamma^m)$ be the mass-lumped L^2–projection of $\vec{\nu}^m$ onto $\underline{V}(\Gamma^m)$, i.e. $\langle \vec{\omega}^m, \vec{\varphi} \rangle^h_{\Gamma^m} = \langle \vec{\nu}^m, \vec{\varphi} \rangle_{\Gamma^m}$ for all $\vec{\varphi} \in \underline{V}(\Gamma^m)$. It is easy to see that $\vec{\omega}^m(\vec{q}^m_k) \neq \vec{0}$ for all $k = 1, \ldots, K_\Gamma$, because Γ^m is the boundary of an open domain. Then it follows from choosing $\vec{\eta} = \vec{\pi}^m[\kappa\, \vec{\omega}^m]$ in (3.8) that

$$0 = \langle \kappa\, \vec{\nu}^m, \vec{\omega}^m \rangle^h_{\Gamma^m} = \langle \vec{\nu}^m, \vec{\pi}^m[\kappa\, \vec{\omega}^m] \rangle_{\Gamma^m} = \langle \vec{\omega}^m, \vec{\pi}^m[\kappa\, \vec{\omega}^m] \rangle^h_{\Gamma^m} = \left\langle \kappa, |\vec{\omega}^m|^2 \right\rangle^h_{\Gamma^m},$$

and so $\kappa = 0 \in W(\Gamma^m)$. Finally, it follows from (3.5a) with $\vec{U} = \vec{0}$ and $\kappa = 0$, on recalling (3.1), that $P = 0$. Hence there exists a unique solution $(\vec{U}^{m+1}, P^{m+1}, \vec{X}^{m+1}, \kappa^{m+1}) \in \mathbb{U}^m \times \widehat{\mathbb{P}}^m \times \underline{V}(\Gamma^m) \times W(\Gamma^m)$ to (3.4a–d). □

3.3 Stability

We now demonstrate that the scheme (3.4a–d) satisfies an energy estimate, which corresponds to the bound (2.9) in the continuous case. In particular, we obtain an unconditional stability result for our scheme.

Theorem 2. *Let $m \in \{0, \ldots, M-1\}$ and let $(\vec{U}^{m+1}, P^{m+1}, \vec{X}^{m+1}, \kappa^{m+1}) \in \mathbb{U}^m \times \widehat{\mathbb{P}}^m \times \underline{V}(\Gamma^m) \times W(\Gamma^m)$ be the unique solution to* (3.4a–d)*. Then*

$$\gamma\, \mathcal{H}^{d-1}(\Gamma^{m+1}) + 2\, \tau_m \left(\mu^m\, \underline{\underline{D}}(\vec{U}^{m+1}), \underline{\underline{D}}(\vec{U}^{m+1}) \right) \leq \gamma\, \mathcal{H}^{d-1}(\Gamma^m) + \tau_m \left(\vec{f}^{m+1}, \vec{U}^{m+1} \right). \tag{3.9}$$

In addition, let $\{t_k\}_{k=0}^M$ be an arbitrary partitioning of $[0,T]$. Then it holds that

$$\gamma\, \mathcal{H}^{d-1}(\Gamma^{m+1}) + 2 \sum_{k=0}^{m} \tau_k \left(\mu^k\, \underline{\underline{D}}(\vec{U}^{k+1}), \underline{\underline{D}}(\vec{U}^{k+1}) \right) \leq \gamma\, \mathcal{H}^{d-1}(\Gamma^0) + \sum_{k=0}^{m} \tau_k \left(\vec{f}^{k+1}, \vec{U}^{k+1} \right) \tag{3.10}$$

for $m = 0, \ldots, M-1$.

Proof. Choosing $\vec{\xi} = \vec{U}^{m+1} \in \mathbb{U}^m$ in (3.4a), $\varphi = P^{m+1} \in \widehat{\mathbb{P}}^m$ in (3.4b), $\chi = \gamma\, \kappa^{m+1}$ in (3.4c) and $\vec{\eta} = \gamma\, (\vec{X}^{m+1} - \vec{\mathrm{id}}|_{\Gamma^m})$ in (3.4d) yields that

$$\begin{aligned} &2\, \tau_m \left(\mu^m\, \underline{\underline{D}}(\vec{U}^{m+1}), \underline{\underline{D}}(\vec{U}^{m+1}) \right) + \gamma \left\langle \nabla_s\, \vec{X}^{m+1}, \nabla_s\, (\vec{X}^{m+1} - \vec{\mathrm{id}}) \right\rangle_{\Gamma^m} \\ &\qquad = \tau_m \left(\vec{f}^{m+1}, \vec{U}^{m+1} \right). \end{aligned}$$

Hence (3.9) follows immediately, where we have used the result that

$$\left\langle \nabla_s \vec{X}^{m+1}, \nabla_s \left(\vec{X}^{m+1} - \vec{\mathrm{id}}\right)\right\rangle_{\Gamma^m} \geq \mathcal{H}^{d-1}(\Gamma^{m+1}) - \mathcal{H}^{d-1}(\Gamma^m)\,,$$

see e.g. [5, Proof of Theorem 2.3] and [6, Proof of Theorem 2.2] for the proofs for $d = 2$ and $d = 3$, respectively. The desired result (3.10) immediately follows from (3.9). □

3.4 Discrete stationary solutions

If the solution $(\vec{U}^{m+1}, P^{m+1}, \vec{X}^{m+1}, \kappa^{m+1})$ to (3.4a–d) is such that the interface has not moved, $\Gamma^{m+1} = \Gamma^m$, then it holds that

$$\exists\, \zeta \in W(\Gamma^m) \;:\quad \langle \zeta\, \vec{\nu}^m, \vec{\eta}\rangle^h_{\Gamma^m} + \left\langle \nabla_s\, \vec{\mathrm{id}}, \nabla_s\, \vec{\eta}\right\rangle_{\Gamma^m} = 0 \quad \forall\ \vec{\eta} \in \underline{V}(\Gamma^m)\,. \tag{3.11}$$

We recall from [5, Remark 2.4] that (3.11) in the case $d = 2$ implies that Γ^m is equidistributed, with the possible exception of elements σ^m_j that are locally parallel to each other; see also [7, Theorem 2.2]. Moreover, we recall from [6, §4.1] that surfaces $\Gamma^m \subset \mathbb{R}^3$ that satisfy (3.11) are called conformal polyhedral surfaces.

Next we consider discrete stationary solutions when no outer forces act, i.e. when $\vec{f} = \vec{0}$. Here, independently of the choice of $\mu_\pm$, no spurious velocities appear for discrete stationary solutions. This is an immediate consequence of Theorem 2, as the following proof shows.

Theorem 3. *Let $(\vec{U}^{m+1}, P^{m+1}, \vec{X}^{m+1}, \kappa^{m+1}) \in \mathbb{U}^m \times \widehat{\mathbb{P}}^m \times \underline{V}(\Gamma^m) \times W(\Gamma^m)$ be the unique solution to* (3.4a–d) *with $\vec{f}^{m+1} = \vec{0}$. If $\Gamma^{m+1} = \Gamma^m$, then $\vec{U}^{m+1} = \vec{0}$.*

Proof. Clearly the solution satisfies (3.9) with Γ^{m+1} replaced by Γ^m and with $\vec{f}^{m+1} = \vec{0}$. Hence we obtain that $(\mu^m\, \underline{\underline{D}}(\vec{U}^{m+1}), \underline{\underline{D}}(\vec{U}^{m+1})) = 0$, and so Korn's inequality implies that $\vec{U}^{m+1} = \vec{0}$. □

In addition, we can prove that discrete stationary solution exist for our scheme.

Theorem 4. *Let $S^m_0 \subset \mathbb{P}^m$ and let $\vec{f}^{m+1} = \vec{0}$. Moreover, let Γ^m be a polyhedral surface with constant discrete mean curvature, i.e. there exists a constant $\overline{\kappa} \in \mathbb{R}$ such that*

$$\overline{\kappa}\, \langle \vec{\nu}^m, \vec{\eta}\rangle_{\Gamma^m} + \left\langle \nabla_s\, \vec{\mathrm{id}}, \nabla_s\ \vec{\eta}\right\rangle_{\Gamma^m} = 0 \quad \forall\, \vec{\eta} \in \underline{V}(\Gamma^m)\,. \tag{3.12}$$

Then Γ^m satisfies (3.11) *and*

$$(\vec{U}^{m+1}, P^{m+1}, \vec{X}^{m+1}, \kappa^{m+1}) = \left(\vec{0}, -\gamma\, \overline{\kappa} \left[\mathcal{X}_{\Omega^m_-} - \frac{\mathcal{L}^d(\Omega^m_-)}{\mathcal{L}^d(\Omega)}\right], \vec{\mathrm{id}}\,|_{\Gamma^m}, \overline{\kappa}\right) \tag{3.13}$$

is the the unique solution to (3.4a–d).

Proof. It immediately follows from (3.12) that (3.11) holds. We now show that the solution stated in (3.13) solves (3.4a–d). Since $\mathcal{X}_{\Omega^m_-} \in \mathbb{P}^m$, we have that $P^{m+1} \in \widehat{\mathbb{P}}^m$, and so (3.13) is

admissible. Clearly, the three equations (3.4b), (3.4c) and (3.4d) hold trivially. In order to show that (3.4a) holds, we observe that the divergence theorem implies that

$$-\gamma \left\langle \kappa^{m+1}\, \vec{\nu}^m, \vec{\xi} \right\rangle_{\Gamma^m} = -\gamma\, \overline{\kappa} \left\langle \vec{\nu}^m, \vec{\xi} \right\rangle_{\Gamma^m} = -\gamma\, \overline{\kappa} \left(\nabla . \vec{\xi}, \mathcal{X}_{\Omega^m_-} \right) = \left(\nabla . \vec{\xi}, P^{m+1} \right)$$

for all $\vec{\xi} \in \mathbb{U}^m$, where we have observed that P^{m+1} differs from $-\gamma\, \overline{\kappa}\, \mathcal{X}_{\Omega^m_-}$ only by a constant. Hence (3.4a) also holds, and so (3.13) is the unique solution to (3.4a–d) □

We remark that in practice we do observe the solution (3.13) for approximations of stationary spherical bubble solutions, see §4.1 and §4.5 for details.

3.5 Semidiscrete scheme

We briefly investigate a semidiscrete variant of the scheme (3.4a–d) in order to highlight two additional important properties of the scheme: a good tangential distribution of mesh points, and good volume conservation.

Let $(\Gamma^h(t))_{t\in[0,T]}$ be a family of polyhedral surfaces, with outer normal $\vec{\nu}^h$. Similarly to (2.1), we can then define the discrete velocity $\vec{\mathcal{V}}^h$, see e.g. [9, (3.3)]. We also define the piecewise linear finite element spaces $W(\Gamma^h(t))$ and $\underline{V}(\Gamma^h(t))$. For $t \in [0,T]$, let $\mathcal{T}^h(t)$ be a regular partitioning of Ω into disjoint open simplices and define the finite element spaces $S^h_k(t)$, $\mathbb{U}^h(t)$ and $\mathbb{P}^h(t)$ similarly to S^m_k, $\mathbb{U}^m$ and $\mathbb{P}^m$, with the corresponding interpolation operators I^h_k and discrete approximations $\mu^h(t) \in S^h_0(t)$. Then, given $\Gamma^h(0)$, for $t \in (0,T]$ find $\Gamma^h(t)$, such that $\vec{\mathcal{V}}^h \in \underline{V}(\Gamma^h(t))$, and $\vec{U}^h(t) \in \mathbb{U}^h(t)$, $P^h(t) \in \widehat{\mathbb{P}}^h(t)$ and $\kappa^h(t) \in W(\Gamma^h(t))$ such that

$$2\left(\mu^h\, \underline{\underline{D}}(\vec{U}^h), \underline{\underline{D}}(\vec{\xi})\right) - \left(P^h, \nabla . \vec{\xi}\right) - \gamma \left\langle \kappa^h\, \vec{\nu}^h, \vec{\xi} \right\rangle_{\Gamma^h(t)} = \left(\vec{f}^h, \vec{\xi}\right) \forall\ \vec{\xi} \in \mathbb{U}^h(t)\,, \tag{3.14a}$$

$$\left(\nabla . \vec{U}^h, \varphi\right) = 0 \quad \forall\ \varphi \in \widehat{\mathbb{P}}^h(t)\,, \tag{3.14b}$$

$$\left\langle \vec{\mathcal{V}}^h, \chi\, \vec{\nu}^h \right\rangle^h_{\Gamma^h(t)} - \left\langle \vec{U}^h, \chi\, \vec{\nu}^h \right\rangle_{\Gamma^h(t)} = 0 \quad \forall\ \chi \in W(\Gamma^h(t))\,, \tag{3.14c}$$

$$\left\langle \kappa^h\, \vec{\nu}^h, \vec{\eta} \right\rangle^h_{\Gamma^h(t)} + \left\langle \nabla_s\, \mathrm{i\vec{d}}, \nabla_s\, \vec{\eta} \right\rangle_{\Gamma^h(t)} = 0 \quad \forall\ \vec{\eta} \in \underline{V}(\Gamma^h(t))\,, \tag{3.14d}$$

where $\vec{f}^h := \vec{I}^h_2\, \vec{f}(t)$.

First of all we note that a solution $\Gamma^h(t)$ to (3.14a–d) clearly satisfies (3.11), with Γ^m replaced by $\Gamma^h(t)$. This means that in 2d the polygonal curve $\Gamma^h(t)$ is equidistributed, and asymptotically this property is inherited by our fully discrete scheme (3.4a–d); see e.g. Figure 6 below. In 3d the property (3.11) means that $\Gamma^h(t)$ is a conformal polyhedral surface, which implies that the mesh quality is good. Once again, we observe in practice that the fully discrete solutions to (3.4a–d) also exhibit nice meshes, without coalescence or other mesh defects occurring.

Secondly, we can show that solutions to (3.14a–d) satisfy a discrete analogue of (2.11). To see this, choose $\chi = 1$ in (3.14c) and $\varphi = (\mathcal{X}_{\Omega^h_-(t)} - \frac{\mathcal{L}^d(\Omega^h_-(t))}{\mathcal{L}^d(\Omega)}) \in \widehat{\mathbb{P}}^h(t)$ in (3.14b), to obtain

$$\begin{aligned}\frac{\mathrm{d}}{\mathrm{d}t}\mathcal{L}^d(\Omega^h_-(t)) &= \left\langle \vec{\mathcal{V}}^h, \vec{\nu}^h \right\rangle_{\Gamma^h(t)} = \left\langle \vec{\mathcal{V}}^h, \vec{\nu}^h \right\rangle^h_{\Gamma^h(t)} = \left\langle \vec{U}^h, \vec{\nu}^h \right\rangle_{\Gamma^h(t)} \\ &= \int_{\Omega^h_-(t)} \nabla \,.\, \vec{U}^h \,\mathrm{d}\mathcal{L}^d = 0\,.\end{aligned}$$

Hence solution to (3.14a–d) conserve the enclosed volume. Once again, the fully discrete scheme (3.4a–d) inherits this property in the sense that in our simulations the volumes are always well maintained.

3.6 Solution method

As is standard practice for the solution of linear systems arising from discretizations of (Navier-)Stokes equations, we avoid the complications of the constrained pressure space $\widehat{\mathbb{P}}^m$ in practice by considering an overdetermined linear system with $\mathbb{P}^m$ instead. In a post-processing step the computed pressure is then projected into the space of zero mean functions. The linear system (3.4a–d), with $\widehat{\mathbb{P}}^m$ replaced by $\mathbb{P}^m$, can be formulated as:

Find $(\vec{U}^{m+1}, P^{m+1}, \kappa^{m+1}, \delta\vec{X}^{m+1})$, where $\vec{X}^{m+1} = \vec{X}^m + \delta\vec{X}^{m+1}$, such that

$$\begin{pmatrix} \vec{B}_\Omega & \vec{C}_\Omega & -\gamma\,\vec{N}_{\Gamma,\Omega} & 0 \\ \vec{C}^T_\Omega & 0 & 0 & 0 \\ \vec{N}^T_{\Gamma,\Omega} & 0 & 0 & -\frac{1}{\tau_m}\vec{N}^T_\Gamma \\ 0 & 0 & \vec{N}_\Gamma & \vec{A}_\Gamma \end{pmatrix} \begin{pmatrix} \vec{U}^{m+1} \\ P^{m+1} \\ \kappa^{m+1} \\ \delta\vec{X}^{m+1} \end{pmatrix} = \begin{pmatrix} \vec{c} \\ 0 \\ 0 \\ -\vec{A}_\Gamma\,\vec{X}^m \end{pmatrix}, \tag{3.15}$$

where $(\vec{U}^{m+1}, P^{m+1}, \kappa^{m+1}, \delta\vec{X}^{m+1}) \in (\mathbb{R}^d)^{K^m_{\mathbb{U}}} \times \mathbb{R}^{K^m_{\mathbb{P}}} \times \mathbb{R}^{K_\Gamma} \times (\mathbb{R}^d)^{K_\Gamma}$ here denote the coefficients of these finite element functions with respect to the standard bases of $\mathbb{U}^m$, $\mathbb{P}^m$, $W(\Gamma^m)$ and $\underline{V}(\Gamma^m)$, respectively. Moreover, $\vec{X}^m$ denotes the coefficients of $\vec{\mathrm{id}}\,|_{\Gamma^m}$ with respect to the basis of $\underline{V}(\Gamma^m)$. The definitions of the matrices and vectors in (3.15) are:

$$\begin{aligned}
&[\vec{B}_\Omega]_{ij} := 2\left(\left(\mu^m\,\underline{\underline{D}}(\phi^{\mathbb{U}^m}_j\,\vec{e}_r), \underline{\underline{D}}(\phi^{\mathbb{U}^m}_i\,\vec{e}_s)\right)\right)^d_{r,s=1}, \quad \vec{c}_i = \left(\vec{f}^{m+1}, \phi^{\mathbb{U}^m}_i\right), \\
&[\vec{C}_\Omega]_{iq} := -\left(\left(\nabla \,.\, (\phi^{\mathbb{U}^m}_i\,\vec{e}_r), \phi^{\mathbb{P}^m}_q\right)\right)^d_{r=1}, \quad [\vec{N}_{\Gamma,\Omega}]_{il} := \left\langle \phi^{\mathbb{U}^m}_i, \chi^m_l\,\vec{\nu}^m \right\rangle_{\Gamma^m}, \\
&[\vec{N}_\Gamma]_{kl} := \langle \chi^m_l, \chi^m_k\,\vec{\nu}^m\rangle^h_{\Gamma^m}, \quad [\vec{A}_\Gamma]_{kl} := \langle \nabla_s\,\chi^m_l, \nabla_s\,\chi^m_k\rangle_{\Gamma^m}\,\vec{\mathrm{id}},
\end{aligned}$$

where $\phi^{\mathbb{U}^m} \in \mathbb{U}^m$, $\phi^{\mathbb{P}^m} \in \mathbb{P}^m$ and $\chi^m \in W(\Gamma^m)$. Note that for the submatrices we have used the convention that the subscripts refer to the test and trial domains, respectively.

For the the solution of (3.15) we use a Schur complement approach that eliminates $(\kappa^{m+1}, \delta\vec{X}^{m+1})$ from (3.15), and then use an iterative solver for the remaining system in $(\vec{U}^{m+1}, P^{m+1})$. This approach has the advantage that for the reduced system well-known solution methods for finite element discretizations for standard (Navier-)Stokes discretizations

may be employed. The desired Schur complement can be obtained as follows. Let

$$\Xi_\Gamma := \begin{pmatrix} 0 & -\frac{1}{\tau_m}\,\vec{N}_\Gamma^T \\ \vec{N}_\Gamma & \vec{A}_\Gamma \end{pmatrix}. \tag{3.16}$$

Then (3.15) can be reduced to

$$\begin{pmatrix} \vec{B}_\Omega + \gamma\,(\vec{N}_{\Gamma,\Omega}\ 0)\,\Xi_\Gamma^{-1}\begin{pmatrix}\vec{N}_{\Gamma,\Omega}^T\\ 0\end{pmatrix} & \vec{C}_\Omega \\ \vec{C}_\Omega^T & 0 \end{pmatrix} \begin{pmatrix} \vec{U}^{m+1} \\ P^{m+1} \end{pmatrix} = \begin{pmatrix} \vec{c} - \gamma\,(\vec{N}_{\Gamma,\Omega}\ 0)\,\Xi_\Gamma^{-1}\begin{pmatrix}0\\ \vec{A}_\Gamma\,\vec{X}^m\end{pmatrix} \\ 0 \end{pmatrix} \tag{3.17a}$$

and

$$\begin{pmatrix} \kappa^{m+1} \\ \delta\vec{X}^{m+1} \end{pmatrix} = \Xi_\Gamma^{-1} \begin{pmatrix} -\vec{N}_{\Gamma,\Omega}^T\,\vec{U}^{m+1} \\ -\vec{A}_\Gamma\,\vec{X}^m \end{pmatrix}. \tag{3.17b}$$

For the solution of (3.17a) we employ a preconditioned GMRES iterative solver, where for the inverse Ξ_Γ^{-1} we employ a sparse $L\,U$ decomposition, which we obtain with the help of the sparse factorization package UMFPACK, see [13].

As preconditioner we use the matrix

$$\mathcal{P} = \begin{pmatrix} \vec{B}_\Omega & \vec{C}_\Omega \\ 0 & -M_\Omega \end{pmatrix}, \tag{3.18}$$

where M_Ω is the pressure mass matrix defined as

$$[M_\Omega]_{ij} = \left(\,\phi_j^{\mathbb{P}^m},\,\phi_i^{\mathbb{P}^m}\right).$$

An application of the preconditioner (3.18) amounts to solving the equations

$$\begin{pmatrix} \vec{B}_\Omega & \vec{C}_\Omega \\ 0 & -M_\Omega \end{pmatrix} \begin{pmatrix} \vec{U} \\ P \end{pmatrix} = \begin{pmatrix} \vec{v} \\ q \end{pmatrix} \iff M_\Omega\,P = -q\,, \quad \vec{B}_\Omega\,\vec{U} = \vec{v} - \vec{C}_\Omega\,P\,.$$

See [16] for more details.

Having obtained $(\vec{U}^{m+1}, P^{m+1})$ from (3.17a), we solve (3.17b) for $(\kappa^{m+1}, \delta\vec{X}^{m+1})$.

Remark 5. *With a view towards some numerical test cases in Section 4, we also allow for an inhomogeneous Dirichlet boundary condition $\vec{g}$ on $\partial\Omega$. In this case the linear system is suitably adjusted. For example, in place of* (3.4b)*, with $\widehat{\mathbb{P}}^m$ replaced by $\mathbb{P}^m$, we require*

$$\left(\nabla\,.\,\vec{U}^{m+1}, \varphi\right) = \frac{(\varphi,1)}{\mathcal{L}^d(\Omega)} \int_{\partial\Omega} (\vec{I}_2^m\,\vec{g})\,.\,\vec{\mathrm{n}}\,\mathrm{d}\mathcal{H}^{d-1} \quad \forall\ \varphi \in \mathbb{P}^m\,. \tag{3.19}$$

3.7 Mesh generation and smoothing

Given the initial polyhedral surface Γ^0, we create a triangulation $\mathcal{T}^0$ of Ω that is fitted to Γ^0 with the help of the package `Gmsh`, see [21]. Then, for $m \geq 0$, having computed the new interface Γ^{m+1}, we would like to obtain a bulk triangulation $\mathcal{T}^{m+1}$ that is fitted to Γ^{m+1}, and

ideally is close to $\mathcal{T}^m$. This is to avoid unnecessary overhead from remeshing the domain Ω completely.

To this end, we perform the following smoothing step on $\mathcal{T}^m$, which is inspired by the method proposed in [18], see also [20]. Having obtained $\delta\vec{X}^{m+1}$ from the solution of (3.15), we solve the linear elasticity problem: Find a displacement $\vec{\psi} \in [H^1(\Omega)]^d$ such that

$$\nabla \,.\, \underline{\underline{S}}(\vec{\psi}) = 0 \qquad \text{in } \Omega^m_\pm\,, \tag{3.20a}$$

$$\vec{\psi} = \delta\vec{X} \qquad \text{on } \Gamma^m\,, \tag{3.20b}$$

$$\vec{\psi}\,.\,\vec{\mathrm{n}} = 0 \qquad \text{on } \partial\Omega\,, \tag{3.20c}$$

where

$$\underline{\underline{S}}(\vec{\psi}) = (\nabla\,.\vec{\psi})\,\underline{\underline{\mathrm{id}}} + 2\,\underline{\underline{D}}(\vec{\psi}) \tag{3.21}$$

is the stress tensor with Lamé moduli $\lambda = \mu = 1$, and where $\vec{\mathrm{n}}$ in (3.20c) is the outer unit normal to Ω on $\partial\Omega$. In practice we approximate (3.20a–c) with piecewise linear elements and solve the resulting system of linear equations with the UMPFACK package, see [13]. The obtained discrete variant of $\vec{\psi}$, at every vertex of the current bulk grid $\mathcal{T}^m$, then represents the variation in their position that we compute in order to obtain $\mathcal{T}^{m+1}$.

Occasionally the deformation of the mesh becomes too large, for instance when the bubble making up the inner phase undergoes strong deformations, and so a complete remeshing of Ω becomes necessary. In order to detect the need for a complete remeshing, we define the criterion

$$\frac{\max_{o\in\mathcal{T}^{m+1}}(\mathcal{H}^d(o))}{\min_{o\in\mathcal{T}^{m+1}}(\mathcal{H}^d(o))} \geq C_r \geq 1, \tag{3.22}$$

where C_r is a fixed constant. Of course, if we choose $C_r = 1$, then a remeshing would be triggered after every time step.

4 Numerical results

We implemented the scheme (3.4a–d) with the help of the toolbox `DUNE`, see [11, 10], using the finite element module `DUNE-FEM`, see [15]. As grid manager we used `ALBERTA`, see [35]. The CPU times which we report are measured in seconds and correspond to a single thread computation on an Intel Xeon E5640 (2.67GHz) processor with 16 GB of main memory.

In order to test our method, and to allow comparisons with the unfitted finite element approximation in [8], we recall the following stationary and expanding spherical solutions from [8]. Firstly, the stationary sphere $\Gamma(t) = \{\vec{z} \in \mathbb{R}^d : |\vec{z}| = r(t)\}$, where

$$r(t) = r(0)\,, \tag{4.1a}$$

together with

$$\vec{u}(\vec{z},t) = \vec{0}\,, \quad p(\vec{z},t) = \lambda(t)\left[\mathcal{X}_{\Omega_-(0)} - \frac{\mathcal{L}^d(\Omega_-(0))}{\mathcal{L}^d(\Omega)}\right], \tag{4.1b}$$

where $\lambda(t) = \lambda(0) = \gamma\,(d-1)\,[r(0)]^{-1}$, is an exact solution to the problem (2.6a–g) on e.g. $\Omega = (-1,1)^d$. Secondly, a nontrivial divergence free and radially symmetric solution $\vec{u}$ can

be constructed on a domain that does not contain the origin. To this end, consider e.g. $\Omega = (-1,1)^d \setminus [-\frac{1}{3},\frac{1}{3}]^d$, and let $\alpha \geq 0$ be given. Then $\Gamma(t) = \{\vec{z} \in \mathbb{R}^d : |\vec{z}| = r(t)\}$, where

$$r(t) = ([r(0)]^d + \alpha\, t\, d)^{\frac{1}{d}}\,, \tag{4.2a}$$

together with

$$\vec{u}(\vec{z},t) = \alpha\,|\vec{z}|^{-d}\,\vec{z}\,, \quad p(\vec{z},t) = \lambda(t)\left[\mathcal{X}_{\Omega_-(t)} - \frac{\mathcal{L}^d(\Omega_-(t))}{\mathcal{L}^d(\Omega)}\right], \tag{4.2b}$$

where $\lambda(t) = \gamma\,(d-1)\,[r(t)]^{-1} + 2\,\alpha\,(d-1)\,(\mu_+ - \mu_-)\,[r(t)]^{-d}$, is an exact solution to the problem (2.6a–g) with the homogeneous right hand side in (2.6c) replaced by $\vec{g}$, where $\vec{g}(\vec{z}) = \alpha\,|\vec{z}|^{-d}\,\vec{z}$. We will refer to (4.1a,b) as the stationary bubble solution, and to (4.2a) as the expanding bubble solution.

In the following, unless otherwise stated, we choose the initial surface $\Gamma(0) = \{\vec{z} \in \mathbb{R}^d : |\vec{z}| = \frac{1}{2}\}$, and we employ uniform time steps $\tau_m = \tau$, $m = 0, \ldots, M-1$.

Finally, we define the errors

$$\|\Gamma^h - \Gamma\|_{L^\infty} := \max_{m=1,\ldots,M} \|\Gamma^m - \Gamma(t_m)\|_{L^\infty}\,, \tag{4.3}$$

where $\|\Gamma^m - \Gamma(t_m)\|_{L^\infty} := \max_{k=1,\ldots,K_\Gamma} \operatorname{dist}(\vec{q}^{\,m}_k, \Gamma(t_m))$,

$$\|\vec{U} - I_2^h\,\vec{u}\|_{L^\infty} := \max_{m=1,\ldots,M} \|U^m - \vec{I}_2^m\,u(\cdot,t_m)\|_{L^\infty(\Omega)}\,,$$

and

$$\|P - p\|_{L^2(\Omega_T)} := \left[\tau \sum_{m=1}^{M} \|P^m - p(\cdot,t_m)\|^2_{L^2(\Omega)}\right]^{\frac{1}{2}},$$

where for the L^2–norms over Ω we employ a quadrature rule of degree k, with $k = 13$ in 2d and $k = 10$ in 3d.

4.1 Convergence tests in 2d

For the true solution (4.1a,b) we choose the domain $\Omega = (-1,1)^2$ and let $\mu = \gamma = 1$. Therefore, the solution reduces to $r(t) = \frac{1}{2}$, $\vec{u}(\cdot,t) = \vec{0}$ and $p(t) = 2\,\mathcal{X}_{\Omega_-(0)} - \frac{\pi}{8}$ for all $t \geq 0$. We approximate this stationary solution on nearly uniform meshes that feature $J_\Gamma = 2^i$, $i = 4, \ldots, 7$, uniform interface elements and $J^0_\Omega = 224$, 1076, 4240, 17194 bulk elements, respectively. We show the initial mesh for $J_\Gamma = 32$ in Figure 2. In addition, we use a uniform time step size $\tau = 10^{-2}$. We compute the discrete solutions to this stationary problem over the time interval $[0,1]$, and report on the errors for the P2–P0 and P2–(P1+P0) elements in Tables 1 and 2, respectively. We can clearly see that the stationary nature of the true solution (4.1a,b) is captured exactly by our numerical method, see also Figure 3 for a visualization of the discrete pressure in the case $J_\Gamma = 32$. This is not surprising given the result of Theorem 4, and the fact that we use an equidistributed approximation Γ^0, which means that (3.12) is satisfied. Of course, since the discrete solution is stationary, neither smoothing nor remeshing is performed

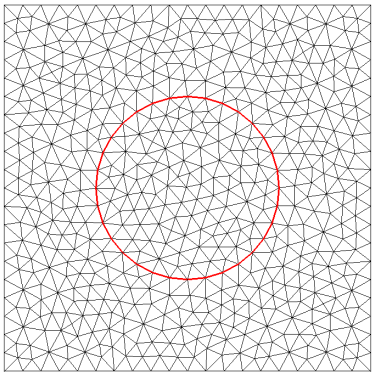

Figure 2: Initial mesh for the 2d stationary bubble problem with $J_\Gamma = 32$ interface elements.

J_Γ	$\|\Gamma^h - \Gamma\|_{L^\infty}$	$\|\vec{U} - I_2^h \vec{u}\|_{L^\infty}$	$\|P - p\|_{L^2(\Omega_T)}$	$CPU[s]$
16	0	0	3.22254e-01	10
32	0	0	1.41195e-01	49
64	0	0	4.06438e-02	378
128	0	0	2.60448e-02	1967

Table 1: ($\mu = \gamma = 1$) Stationary bubble problem on $(-1, 1)^2$ over the time interval $[0, 1]$ for the P2–P0 element.

J_Γ	$\|\Gamma^h - \Gamma\|_{L^\infty}$	$\|\vec{U} - I_2^h \vec{u}\|_{L^\infty}$	$\|P - p\|_{L^2(\Omega_T)}$	$CPU[s]$
16	0	0	3.22254e-01	41
32	0	0	1.41195e-01	821
64	0	0	4.06438e-02	8971
128	0	0	2.60448e-02	55629

Table 2: ($\mu = \gamma = 1$) Stationary bubble problem on $(-1, 1)^2$ over the time interval $[0, 1]$ for the P2–(P1+P0) element.

for the simulations in Tables 1 and 2. We also observe that the error for the two approximations with the P2–P0 and the P2–(P1+P0) element, respectively, produce identical errors. Again, that is to be expected, since the solution (3.13) is such that $P^{m+1} \in S_0^m$, and so the additional degrees of freedom in the space S_1^m are not utilized by the pressure approximation.

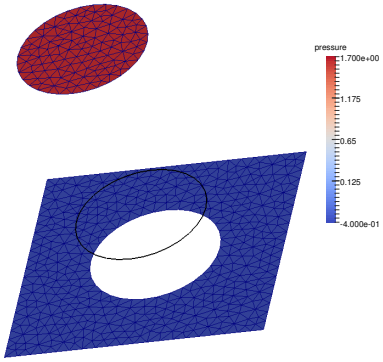

Figure 3: ($\mu = \gamma = 1$) Pressure of the 2d stationary bubble at time $t = 1$ for the P2–P0 element.

For the expanding bubble test, we fix $\Omega = (-1, 1)^2 \setminus [-\frac{1}{3}, \frac{1}{3}]^2$ and we choose the parameters $\alpha = 0.15$ and $\mu_+ = 10\,\mu_- = \gamma = 1$ for the true solution (4.2a,b). Here we consider two different bulk mesh strategies. Either we use a nearly uniform mesh, as shown on the left of Figure 4, or an adaptive mesh that uses a finer resolution close to the interface, see the example mesh on the right hand side of Figure 4.

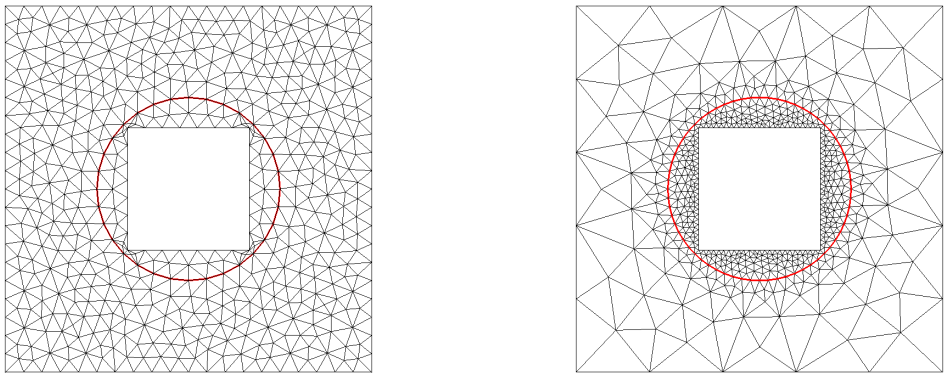

Uniform mesh with $J_\Gamma = 32$ Adaptive mesh with $J_\Gamma = 64$

Figure 4: Initial meshes for the expanding bubble problem.

Details on the discretization parameters for the nearly uniform meshes are given in Table 3.

J_Γ	J_Ω^0	τ	J_Ω^M for $C_r = 1$
16	212	$1.6 \cdot 10^{-2}$	120
32	988	$4 \cdot 10^{-3}$	452
64	3776	10^{-3}	1864

Table 3: Discretization parameters for the 2d expanding bubble problem, uniform meshes.

J_Γ	$\|\Gamma^h - \Gamma\|_{L^\infty}$	$\|\vec{U} - I_2^h \vec{u}\|_{L^\infty}$	$\|P - p\|_{L^2(\Omega_T)}$	$CPU[s]$
16	5.98661e-03	3.67780e-03	4.17354e-01	253
32	1.47669e-03	1.68775e-03	2.29737e-01	5348
64	3.68788e-04	5.35566e-04	1.05960e-01	107430

Table 4: ($\mu_+ = 10\,\mu_- = \gamma = 1, \alpha = 0.15$) Expanding bubble problem on $(-1,1)^2 \setminus [-\frac{1}{3}, \frac{1}{3}]^2$ over the time interval $[0,1]$ for the P2–P0 element, no remeshing and uniform mesh.

Here we explicitly state the final number of bulk elements, J_Ω^M, only in the case $C_r = 1$, recall (3.22), i.e. when the bulk is remeshed after every time step. Of course, when only smoothing is employed, then the number of bulk mesh elements is invariant, and so $J_\Omega^M = J_\Omega^0$. We report on the error for the P2–P0 element, when only mesh smoothings are applied, in Table 4. Due to the expanding motion of the interface, we observe that over time bulk mesh elements strongly deform. This leads to large CPU times and additional approximation errors. Hence, as a comparison, we show the errors for the same element, when the bulk mesh is remeshed after every time step, in Table 5. We observe a dramatic improvement in the CPU times, and a significant reduction in the error quantities. That is why for the P2–(P1+P0) element we only consider the case $C_r = 1$, see Table 6. Comparing the errors in Tables 5 and 6 we note slightly larger CPU times for the latter, which is not surprising, and slightly larger error quantities. It is for this reason that for all the remaining numerical computations we will only consider the P2–P0 element.

The evolution of the discrete pressure solution in the case $J_\Gamma = 32$, for the run with $C_r = 1$, can be seen in Figure 5. Here we note that the discontinuous jump in the pressure at the interface is captured very well, with no oscillations being present. This is a significant improvement on the oscillations observed in the discrete pressures for the unfitted finite element approximation from [8], see e.g. Figure 6 in that paper.

Finally, we would also like to investigate the effect of using adaptive bulk meshes, that are

J_Γ	$\|\Gamma^h - \Gamma\|_{L^\infty}$	$\|\vec{U} - I_2^h \vec{u}\|_{L^\infty}$	$\|P - p\|_{L^2(\Omega_T)}$	$CPU[s]$
16	5.92892e-03	3.86458e-03	4.43308e-01	243
32	1.46653e-03	8.73181e-04	2.14625e-01	4362
64	3.65445e-04	1.92670e-04	8.09743e-02	78947

Table 5: ($\mu_+ = 10\,\mu_- = \gamma = 1, \alpha = 0.15$) Expanding bubble problem on $(-1,1)^2 \setminus [-\frac{1}{3}, \frac{1}{3}]^2$ over the time interval $[0,1]$ for the P2–P0 element, with remeshing at every time step and uniform mesh.

J_Γ	$\|\Gamma^h - \Gamma\|_{L^\infty}$	$\|\vec{U} - I_2^h \vec{u}\|_{L^\infty}$	$\|P - p\|_{L^2(\Omega_T)}$	$CPU[s]$
16	5.95691e-03	4.04415e-03	4.44634e-01	258
32	1.47266e-03	3.23973e-03	2.14906e-01	4683
64	3.65596e-04	2.72450e-04	8.10807e-02	129910

Table 6: ($\mu_+ = 10\,\mu_- = \gamma = 1, \alpha = 0.15$) Expanding bubble problem on $(-1,1)^2 \setminus [-\frac{1}{3}, \frac{1}{3}]^2$ over the time interval $[0,1]$ for the P2–(P1+P0) element, with remeshing at every time step and uniform mesh.

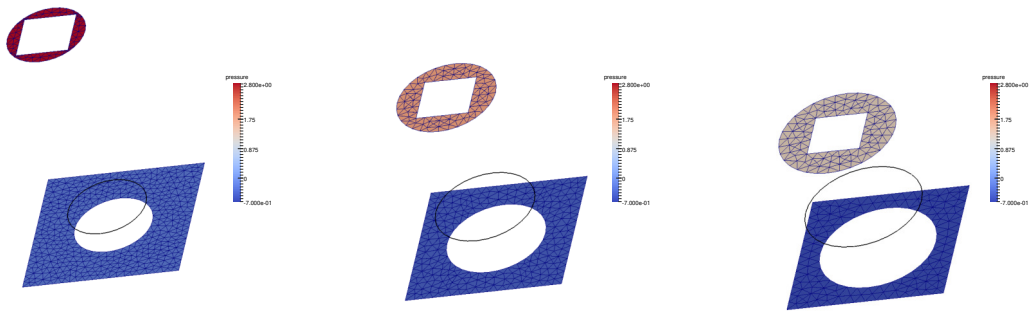

$t = 0$ $t = 0.5$ $t = 1$

Figure 5: ($\mu_+ = 10\,\mu_- = \gamma = 1, \alpha = 0.15$) Pressure evolution of the 2d expanding bubble for the P2–P0 element, uniform mesh.

refined close to the interface. An example mesh is shown on the right hand side of Figure 4, and we list our employed discretization parameters in Table 7. The observed errors for our numerical approximation are shown in Table 8. Comparing the error quantities in Tables 5 and 8 we note that there appears to be no advantage in using a highly refined mesh near the moving interface.

4.2 Equidistribution property in 2d

We now demonstrate the remarkable equidistribution property of our method showing that the circular, equidistributed numerical steady state solution is recovered by our method even if we choose a very nonuniform initial interface Γ^0. In particular, for the presented numerical simulation, we take Γ^0 to be a very nonuniform approximation of a unit circle, where we

J_Γ	J_Ω^0	τ	J_Ω^M
32	584	$6.4 \cdot 10^{-2}$	234
64	1020	$1.6 \cdot 10^{-2}$	564
128	2506	$4 \cdot 10^{-3}$	1226
256	7460	10^{-3}	3872

Table 7: Discretization parameters for the 2d expanding bubble problem, adaptive meshes.

J_Γ	$\|\Gamma^h - \Gamma\|_{L^\infty}$	$\|\vec{U} - I_2^h \vec{u}\|_{L^\infty}$	$\|P - p\|_{L^2(\Omega_T)}$	$CPU[s]$
32	3.91426e-03	1.86979e-03	5.57560e-01	97
64	9.96943e-04	1.83143e-03	2.94448e-01	590
128	2.51524e-04	2.63245e-03	1.51500e-01	11003
256	6.04565e-05	6.90220e-04	6.32413e-02	130320

Table 8: ($\mu_+ = 10\,\mu_- = \gamma = 1, \alpha = 0.15$) Expanding bubble problem on $(-1,1)^2 \setminus [-\frac{1}{3},\frac{1}{3}]^2$ over the time interval $[0,1]$ for the P2–P0 element, with remeshing at every time step and adaptive mesh.

represent the upper half of the circle by a single vertex, while the lower half resembles a semicircle. In total we use $J_\Gamma = 32$ elements for Γ^0 and we start with a very nonuniform bulk mesh with $J_\Omega^0 = 670$ elements. Of course, the initial bulk mesh has to respect the nonuniform approximation of the interface, and so is very nonuniform itself. However, we see from the evolution in Figure 6 that as the interface gets closer and closer to an equidistributed approximation of a circle, the bulk mesh also becomes more uniform. For the presented simulation we used the physical parameters $\mu = \gamma = 1$. The uniform time step size is chosen as $\tau = 10^{-4}$ and we set $C_r = 3$, recall (3.22).

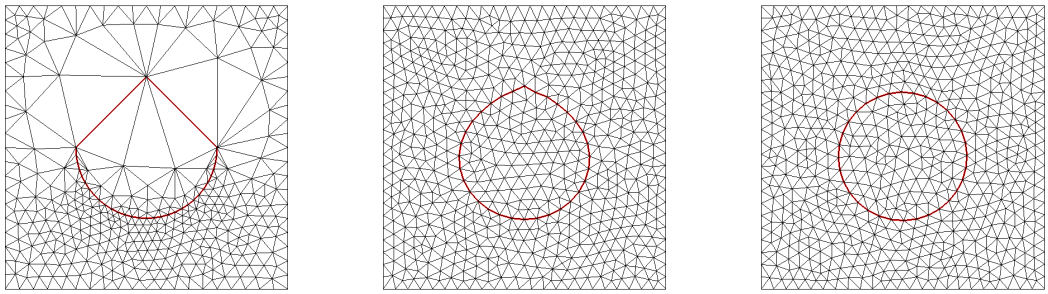

$t = 0$ $t = 1$ $t = 5$

Figure 6: ($\mu = \gamma = 1$) Mesh evolution of a nonuniform circle formed by $J_\Gamma = 32$ elements. Here we use the P2–P0 element, and let $C_r = 3$.

4.3 Energy decay and area conservation in 2d

In Figure 7 we show the pressure evolution for a simulation that starts with an initial ellipse, with major and minor axes of 1.6 and 0.75. The domain is given by $\Omega = (-1,1)^2$ and we use the parameters $\mu = \gamma = 1$, $\tau = 10^{-2}$ and $T = 10$. The initial interface is discretized with $J_\Gamma = 40$ surface elements, and the initial bulk mesh has $J_\Omega^0 = 1112$ elements. We employ the P2–P0 element and use the remeshing parameter $C_r = 3$ during the evolution. Figure 8 shows the evolution of the relative inner area $\frac{\mathcal{L}^2(\Omega_-^m)}{\mathcal{L}^2(\Omega_-^0)}$ and the evolution of the interface energy $\gamma\,\mathcal{H}^1(\Gamma^m)$. The graphs show that the inner area is nearly conserved, and that the interface energy is monotonically decreasing.

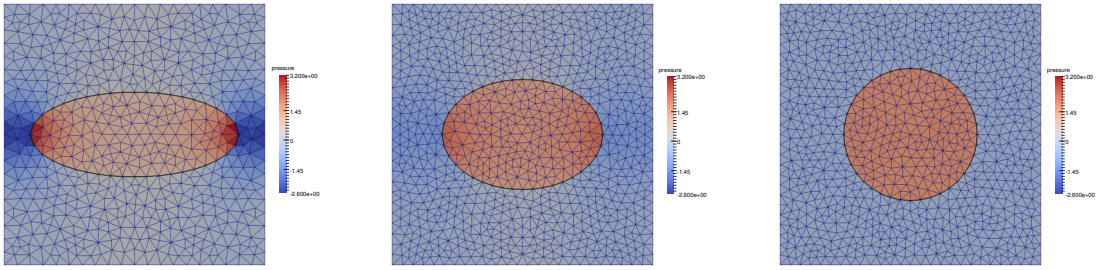

$t = 10^{-5}$ $t = 2.5$ $t = 10$

Figure 7: ($\mu = \gamma = 1$) Pressure evolution of an ellipse that evolves towards a circle. Here we use the P2–P0 element, and let $C_r = 3$.

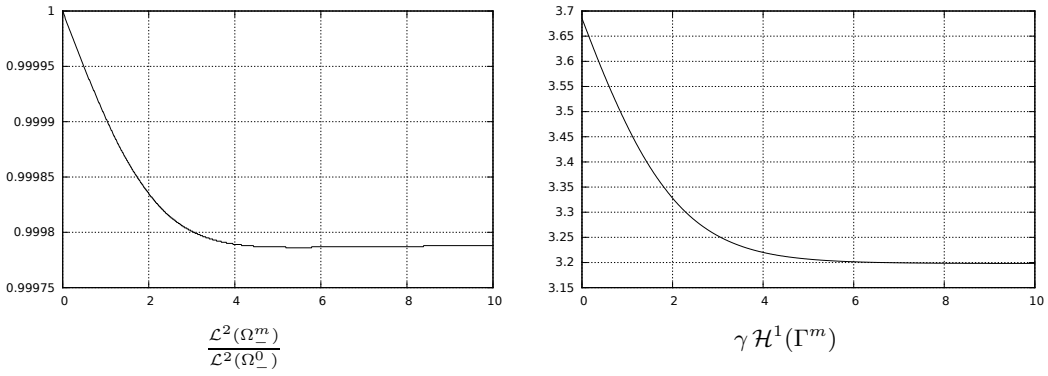

Figure 8: Evolutions of the relative inner area and the interface energy for the simulation in Figure 7.

As a comparison, we show in Figure 9 the final snapshot of the same simulation when no remeshings are performed, i.e. we use $C_r = \infty$ in (3.22). We clearly see that due to the strong deformation of the interface, this leads to elongated elements in the inner and in the outer phase of the bulk finite element mesh.

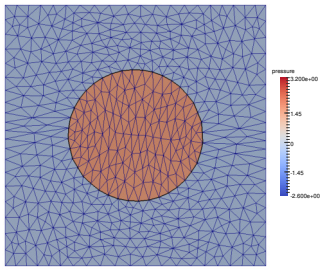

$t = 10$

Figure 9: ($\mu = \gamma = 1$) Final pressure solution for a simulation as in Figure 7, when no remeshings are performed.

4.4 Shear flow experiment in 2d

As the final 2d numerical simulation we present a shear flow experiment in the domain $\Omega = (-1, 1)^2$, with a circle of radius $r = 0.5$ as the initial interface. Here we prescribe the inhomogeneous Dirichlet boundary condition

$$\vec{g}(\vec{z}) = (z_2, 0)^T \quad \text{on } \partial\Omega\,,$$

and we use the parameters $\mu = 1$, $\gamma = 3$, $\tau = 10^{-2}$ and $T = 5$. The initial interface is discretized with $J_\Gamma = 64$ surface elements, and the initial bulk mesh has $J_\Omega^0 = 4240$ elements. In Figure 10 we show the evolution of the discrete pressures for a simulation with $C_r = 3$ for the P2–P0 element, while the velocities are visualized in Figure 11.

4.5 Convergence test in 3d

Similarly to §4.1, we perform the following convergence test for a stationary spherical bubble in 3d. Let $\Omega = (-1, 1)^3$ and $\mu = \gamma = 1$. Then the true solution (4.1a,b) reduces to $r(t) = \frac{1}{2}$, $\vec{u}(\cdot, t) = \vec{0}$ and $p(t) = 4\,\mathcal{X}_{\Omega_-(0)} - \frac{\pi}{12}$ for all $t \geq 0$. We approximate this stationary solution on nearly uniform meshes that feature $J_\Gamma = 32$, 220 and 596 interface elements, and $J_\Omega^0 = 408$, 3590 and 20473 bulk elements, respectively. Here, in contrast to the situation in 2d, we are not able to define Γ^0 such that the vertices of Γ^0 lie on $\Gamma(0)$ and such that (3.12) is satisfied. As we would like to demonstrate the ability of our method to recover the discrete stationary solution (3.13) also in 3d, we choose the initial interface Γ^0 such that (3.12) holds, at the expense of a nonzero initial error $\|\Gamma^0 - \Gamma(0)\|_{L^\infty}$, recall (4.3). We obtain such an initial triangulation with the help of the numerical scheme from [6] for surface diffusion, which is a gradient flow for surface area that maintains the enclosed volume. See e.g. [6, Fig. 11] for an evolution towards

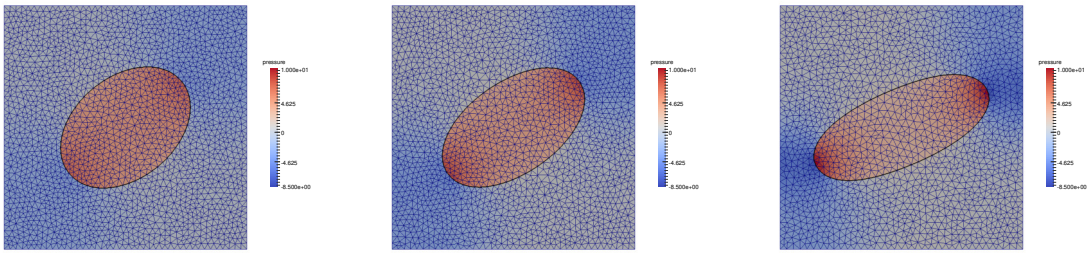

$t = 0.5$ $t = 1$ $t = 5$

Figure 10: $(\mu = 1, \gamma = 3)$ Pressure evolution for the 2d shear flow with $C_r = 3$ for the P2–P0 element, uniform mesh.

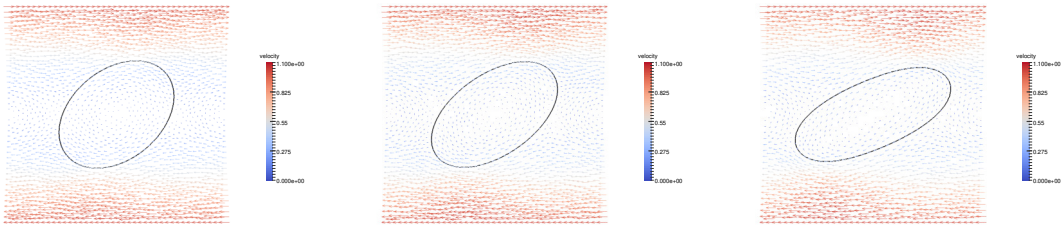

$t = 0.5$ $t = 1$ $t = 5$

Figure 11: $(\mu = 1, \gamma = 3)$ Velocity vector field for the 2d shear flow with $C_r = 3$ for the P2–P0 element, uniform mesh.

J_Γ	$\|\Gamma^h - \Gamma\|_{L^\infty}$	$\|\vec{U} - I_2^h \vec{u}\|_{L^\infty}$	$\|P - p\|_{L^2(\Omega_T)}$	$CPU[s]$
32	2.97986e-02	0	1.65555e-00	385
220	5.80971e-03	0	7.14269e-01	4699
596	2.42857e-03	0	3.58466e-01	51604

Table 9: ($\mu = \gamma = 1$) Stationary bubble problem on $(-1,1)^3$ over the time interval $[0,1]$ for the P2–P0 element.

J_Γ	$\|\Gamma^h - \Gamma\|_{L^\infty}$	$\|\vec{U} - I_2^h \vec{u}\|_{L^\infty}$	$\|P - p\|_{L^2(\Omega_T)}$	$CPU[s]$
32	2.97986e-02	0	1.65749e-00	568
220	5.80971e-03	0	7.15353e-01	9174
596	2.42857e-03	0	3.59181e-01	121110

Table 10: ($\mu = \gamma = 1$) Stationary bubble problem on $(-1,1)^3$ over the time interval $[0,1]$ for the P2–(P1+P0) element.

a polyhedral approximation of a sphere that satisfies (3.12), and hence also (3.11). We report the errors for the P2–P0 element in Table 9, while Table 10 shows the same errors for the P2–(P1+P0) element. In both cases we use the uniform time step size $\tau = 10^{-2}$.

We note that we again recover the discrete stationary solutions (3.13). Here this leads to a nonzero error in the position of the discrete interface, because the vertices of the initial interface Γ^0 do not lie on $\Gamma(0)$.

4.6 Shear flow experiment in 3d

Finally, we also report on a shear flow experiment in the domain $\Omega = (-1,1)^3$, with a sphere of radius $r = 0.5$ as the initial interface. The initial interface mesh has $J_\Gamma = 596$ elements, while the nearly uniform bulk mesh is made up of $J_\Omega^0 = 19641$ elements. We prescribe the inhomogeneous Dirichlet boundary condition

$$\vec{g}(\vec{z}) = (z_3, 0, 0)^T \quad \text{on } \partial\Omega\,,$$

and we use the parameters $\mu = 1$, $\gamma = 3$, $\tau = 10^{-2}$ and $T = 5$. In Figure 12 we show the evolution of the discrete interface for a simulation with $C_r = 3$ for the P2–P0 element, while the velocities are visualized in Figure 13.

A plot of the relative inner volume over time is shown in Figure 14, where we again observe that our numerical method maintains the enclosed volume well.

5 Conclusion

We have presented a novel fitted finite element approximation for two–phase Stokes flow. The method uses a piecewise linear approximation of the interface and employs standard velocity and pressure finite element spaces in the bulk.

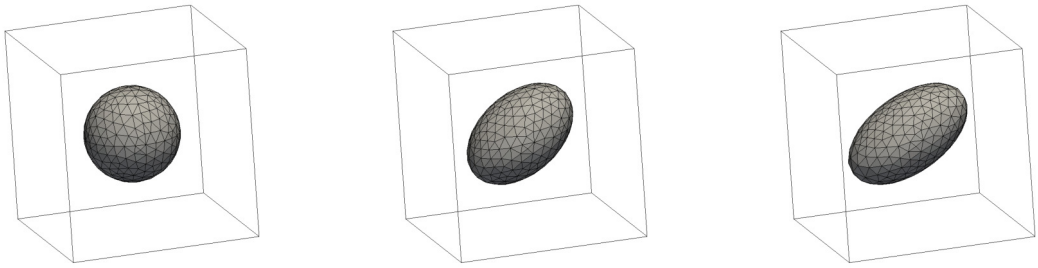

$t = 0$ $t = 1$ $t = 5$

Figure 12: $(\mu = 1, \gamma = 3)$ Interface evolution for the 3d shear flow with $C_r = 3$ for the P2–P0 element, uniform mesh.

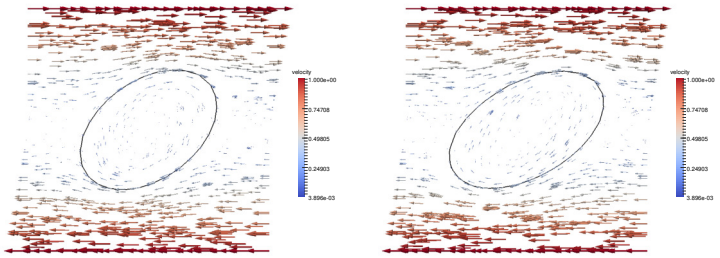

$t = 1$ $t = 5$

Figure 13: $(\mu = 1, \gamma = 3)$ Velocity vector field in the plane normal to $(0, 1, 0)^T$ and passing through the origin for the 3d shear flow with $C_r = 3$ for the P2–P0 element, uniform mesh.

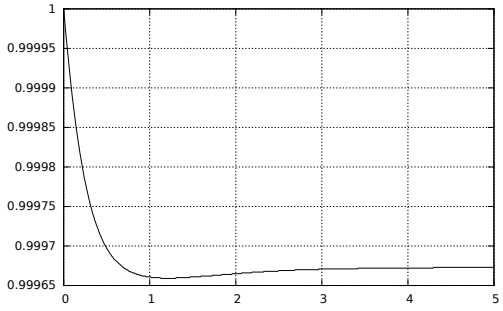

Figure 14: A plot of the relative inner volume $\frac{\mathcal{L}^3(\Omega_-^m)}{\mathcal{L}^3(\Omega_-^0)}$ over time for the simulation in Figure 12.

The scheme is unconditionally stable and can capture simple stationary solutions exactly, which means that no spurious velocities appear. In addition, the discontinuous pressure jumps are captured well in general situations, and no pressure oscillations appear in practice.

Moreover, the numerical solutions exhibit good volume conservation properties and the quality of the interface mesh does not deteriorate in time.

6 Future work

The future work will be the generalization of the FEM fitted scheme described above for a two-phase Navier-Stokes flow. Therefore, instead of having the Stokes flow (2.3a–b), the governing equation will be

$$\rho\,(\vec{u}_t + (\vec{u}\,.\,\nabla)\,\vec{u}) - \nabla\,.\,\underline{\underline{\sigma}} = \rho\,\vec{f} \qquad \text{in } \Omega_\pm(t)\,, \tag{6.1a}$$

$$\nabla\,.\,\vec{u} = 0 \qquad \text{in } \Omega_\pm(t)\,, \tag{6.1b}$$

where $\rho(t) = \rho_+\,\mathcal{X}_{\Omega_+(t)} + \rho_-\,\mathcal{X}_{\Omega_-(t)}$, with $\rho_\pm \in \mathbb{R}_{>0}$, denotes the densities in the two phases.

As preliminary result, it is used the first benchmark problem described in [27], ie. the rectangular domain $\Omega = (0,1) \times (0,2)$ and homogeneous Dirichlet boundary condition on $[0,1] \times \{0,2\}$ and free-slip boundary conditions on $\{0,1\} \times (0,2)$.

The initial interface is the circle $\Gamma_0 = \{\vec{z} \in \mathbb{R}^2 : |\vec{z} - (\frac{1}{2},\frac{1}{2})^T| = \frac{1}{4}\}$ and the physical parameters are

$$\rho_+ = 1000\,, \quad \rho_- = 100\,, \quad \mu_+ = 10\,, \quad \mu_- = 1\,, \quad \gamma = 24.5\,. \tag{6.2}$$

Finally the gravity term is $\vec{f} = (0, -0.98)^T$, the time interval chosen for the simulation is $[0,3]$ and $\tau = 10^{-3}$.

In Figure 15 it is shown the evolution of the velocity vector field and in Figure 16 it is visualized the mesh evolution. The element used is P2–P0 with remeshing at every time step and uniform mesh.

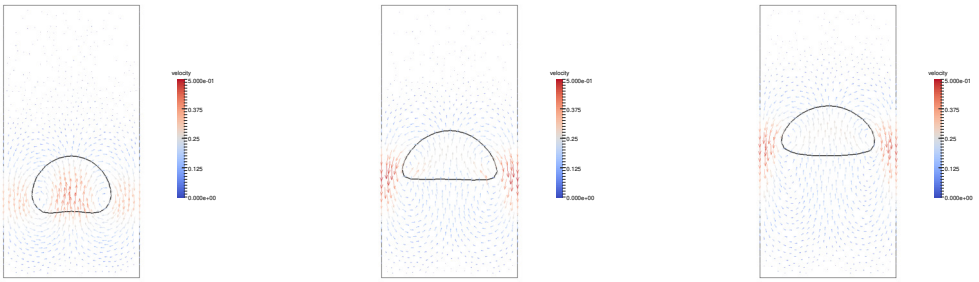

$t = 1$ $t = 2$ $t = 3$

Figure 15: $(\mu_+ = 1000, \mu_- = 100, \rho_+ = 10, \rho_- = 1, \gamma = 24.5)$ Velocity vector field for the 2d rising bubble with with remeshing at every time step for the P2–P0 element, uniform mesh.

The main points which need to be addressed can be summarized as follows.

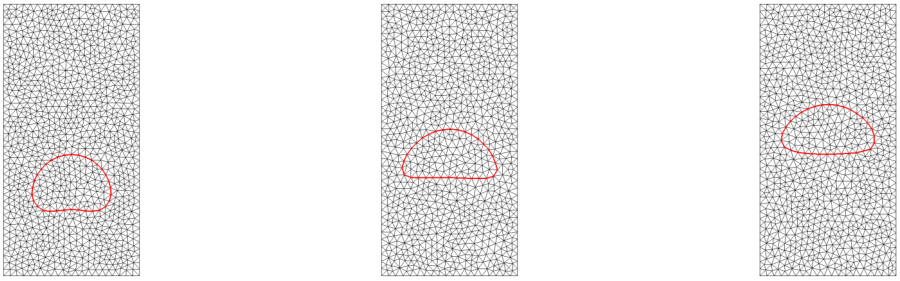

$t = 1$ $t = 2$ $t = 3$

Figure 16: ($\mu_+ = 1000, \mu_- = 100, \rho_+ = 10, \rho_- = 1, \gamma = 24.5$) Mesh evolution for the 2d rising bubble with with remeshing at every time step for the P2–P0 element, uniform mesh.

- Investigate whether the stability proof in Theorem 2 can be extended to Navier-Stokes.
- Implement a new scheme based on Arbitrary Lagrangian Eulerian (ALE) approach. Here a prescribed flow drives the movement of the bulk mesh vertices, and this prescribed flow needs to be accounted for in the approximation of the momentum equation. The movement of the bulk mesh is incorporated in the finite element approximation therefore it avoids the repeated interpolation onto the bulk mesh.
- Investigate whether the stability proof in Theorem 2 can be extended also to the ALE scheme.
- Test other solvers/preconditioners to solve the algebraic linear system more efficiently.
- Include surface active agents (surfactants) to the model. Surfactants molecules can attach to and detach from the interface therefore they influence the surface tension and the corresponding mass balances on the interface and in the bulk have to be taken into account. The fundamental transport mechanisms for surfactants are diffusion in the bulk phases and on the interface, and advection with the underlying fluid velocity.
- Use adaptive meshes to increase the accuracy of the scheme.
- Test higher order spaces to approximate the displacement of the interface.

7 Courses

7.1 Courses for academic credits

During the first two years of my Ph.D. I took the following courses:

- *Manifolds*, Master Course, 30 hours;
- *Theory of PDE's*, TCC, 20 hours;

- *Advanced Finite Element Theory*, TCC, 20 hours;
- *Pseudo Differential Operators*, TCC, 20 hours;
- *Analysis of Points and Lines*, TCC, 20 hours;

completing 110 hours over the 100 hours of compulsory classes.

7.2 Courses for Graduate School

In compliance with College regulations about Transferable Skills, I attended four courses given by the Graduate School, precisely the following:

- *Research Skills & Development*, (RSD) Course, 3 courses;
- *Negotiation Skills for Researchers*, 1 course.

Moreover, I have completed the *Plagiarism Awareness* course and I have met College Postgraduate Research English requirement.

References

[1] H. Abels, H. Garcke, and G. Grün, *Thermodynamically consistent, frame indifferent diffuse interface models for incompressible two-phase flows with different densities*, Math. Models Methods Appl. Sci., 22 (2012), p. 1150013.

[2] M. Agnese and R. Nürnberg, *Fitted finite element discretization of two-phase Stokes flow*, Internat. J. Numer. Methods Fluids, 82 (2016), pp. 709–729.

[3] D. M. Anderson, G. B. McFadden, and A. A. Wheeler, *Diffuse-interface methods in fluid mechanics*, in Annual review of fluid mechanics, Vol. 30, Annual Reviews, Palo Alto, CA, 1998, pp. 139–165.

[4] E. Bänsch, *Finite element discretization of the Navier–Stokes equations with a free capillary surface*, Numer. Math., 88 (2001), pp. 203–235.

[5] J. W. Barrett, H. Garcke, and R. Nürnberg, *A parametric finite element method for fourth order geometric evolution equations*, J. Comput. Phys., 222 (2007), pp. 441–462.

[6] ——, *On the parametric finite element approximation of evolving hypersurfaces in* $\mathbb{R}^3$, J. Comput. Phys., 227 (2008), pp. 4281–4307.

[7] ——, *The approximation of planar curve evolutions by stable fully implicit finite element schemes that equidistribute*, Numer. Methods Partial Differential Equations, 27 (2011), pp. 1–30.

[8] ——, *Eliminating spurious velocities with a stable approximation of viscous incompressible two-phase Stokes flow*, Comput. Methods Appl. Mech. Engrg., 267 (2013), pp. 511–530.

[9] ——, *On the stable numerical approximation of two-phase flow with insoluble surfactant*, M2AN Math. Model. Numer. Anal., 49 (2015), pp. 421–458.

[10] P. Bastian, M. Blatt, A. Dedner, C. Engwer, R. Klöfkorn, R. Kornhuber, M. Ohlberger, and O. Sander, *A Generic Grid Interface for Parallel and Adaptive Scientific Computing. Part II: Implementation and Tests in DUNE*, Computing, 82 (2008), pp. 121–138.

[11] P. Bastian, M. Blatt, A. Dedner, C. Engwer, R. Klöfkorn, M. Ohlberger, and O. Sander, *A Generic Grid Interface for Parallel and Adaptive Scientific Computing. Part I: Abstract Framework*, Computing, 82 (2008), pp. 103–119.

[12] D. Boffi, N. Cavallini, F. Gardini, and L. Gastaldi, *Local mass conservation of Stokes finite elements*, J. Sci. Comput., 52 (2012), pp. 383–400.

[13] T. A. Davis, *Algorithm 832: UMFPACK V4.3—an unsymmetric-pattern multifrontal method*, ACM Trans. Math. Software, 30 (2004), pp. 196–199.

[14] K. Deckelnick, G. Dziuk, and C. M. Elliott, *Computation of geometric partial differential equations and mean curvature flow*, Acta Numer., 14 (2005), pp. 139–232.

[15] A. Dedner, R. Klöfkorn, M. Nolte, and M. Ohlberger, *A Generic Interface for Parallel and Adaptive Scientific Computing: Abstraction Principles and the DUNE-FEM Module*, Computing, 90 (2010), pp. 165–196.

[16] H. C. Elman, D. J. Silvester, and A. J. Wathen, *Finite elements and fast iterative solvers: with applications in incompressible fluid dynamics*, Numerical Mathematics and Scientific Computation, Oxford University Press, New York, 2005.

[17] X. Feng, *Fully discrete finite element approximations of the Navier–Stokes–Cahn–Hilliard diffuse interface model for two-phase fluid flows*, SIAM J. Numer. Anal., 44 (2006), pp. 1049–1072.

[18] S. Ganesan, *Finite element methods on moving meshes for free surface and interface flows*, PhD thesis, University Magdeburg, Magdeburg, Germany, 2006.

[19] S. Ganesan, G. Matthies, and L. Tobiska, *On spurious velocities in incompressible flow problems with interfaces*, Comput. Methods Appl. Mech. Engrg., 196 (2007), pp. 1193–1202.

[20] S. Ganesan and L. Tobiska, *An accurate finite element scheme with moving meshes for computing 3D-axisymmetric interface flows*, Internat. J. Numer. Methods Fluids, 57 (2008), pp. 119–138.

[21] C. Geuzaine and J.-F. Remacle, *Gmsh: A 3-D finite element mesh generator with built-in pre- and post-processing facilities*, Internat. J. Numer. Methods Engrg., 79 (2009), pp. 1309–1331.

[22] V. Girault and P.-A. Raviart, *Finite element methods for Navier–Stokes equations*, vol. 5 of Springer Series in Computational Mathematics, Springer-Verlag, Berlin, 1986. Theory and algorithms.

[23] S. Gross and A. Reusken, *An extended pressure finite element space for two-phase incompressible flows with surface tension*, J. Comput. Phys., 224 (2007), pp. 40–58.

[24] G. Grün and F. Klingbeil, *Two-phase flow with mass density contrast: Stable schemes for a thermodynamic consistent and frame-indifferent diffuse-interface model*, J. Comput. Phys., 257 (2014), pp. 708–725.

[25] C. W. Hirt and B. D. Nichols, *Volume of fluid (VOF) method for the dynamics of free boundaries*, J. Comput. Phys., 39 (1981), pp. 201–225.

[26] P. C. Hohenberg and B. I. Halperin, *Theory of dynamic critical phenomena*, Rev. Mod. Phys., 49 (1977), pp. 435–479.

[27] S. Hysing, S. Turek, D. Kuzmin, N. Parolini, E. Burman, S. Ganesan, and L. Tobiska, *Quantitative benchmark computations of two-dimensional bubble dynamics*, Internat. J. Numer. Methods Fluids, 60 (2009), pp. 1259–1288.

[28] D. Kay, V. Styles, and R. Welford, *Finite element approximation of a Cahn–Hilliard–Navier–Stokes system*, Interfaces Free Bound., 10 (2008), pp. 15–43.

[29] R. J. LeVeque and Z. Li, *Immersed interface methods for Stokes flow with elastic boundaries or surface tension*, SIAM J. Sci. Comput., 18 (1997), pp. 709–735.

[30] J. Lowengrub and L. Truskinovsky, *Quasi-incompressible Cahn–Hilliard fluids and topological transitions*, R. Soc. Lond. Proc. Ser. A Math. Phys. Eng. Sci., 454 (1998), pp. 2617–2654.

[31] S. Osher and R. Fedkiw, *Level Set Methods and Dynamic Implicit Surfaces*, vol. 153 of Applied Mathematical Sciences, Springer-Verlag, New York, 2003.

[32] C. S. Peskin, *The immersed boundary method*, Acta Numer., 11 (2002), pp. 479–517.

[33] S. Popinet, *An accurate adaptive solver for surface-tension-driven interfacial flows*, J. Comput. Phys., 228 (2009), pp. 5838–5866.

[34] Y. Renardy and M. Renardy, *PROST: a parabolic reconstruction of surface tension for the volume-of-fluid method*, J. Comput. Phys., 183 (2002), pp. 400–421.

[35] A. Schmidt and K. G. Siebert, *Design of Adaptive Finite Element Software: The Finite Element Toolbox ALBERTA*, vol. 42 of Lecture Notes in Computational Science and Engineering, Springer-Verlag, Berlin, 2005.

[36] J. A. Sethian, *Level Set Methods and Fast Marching Methods*, Cambridge University Press, Cambridge, 1999.

[37] M. Sussman, P. Semereka, and S. Osher, *A level set approach for computing solutions to incompressible two-phase flow*, J. Comput. Phys., 114 (1994), pp. 146–159.

[38] G. Tryggvason, B. Bunner, A. Esmaeeli, D. Juric, N. Al-Rawahi, W. Tauber, J. Han, S. Nas, and Y.-J. Jan, *A front-tracking method for the computations of multiphase flow*, J. Comput. Phys., 169 (2001), pp. 708–759.

[39] S. O. Unverdi and G. Tryggvason, *A front-tracking method for viscous, incompressible multi-fluid flows*, J. Comput. Phys., 100 (1992), pp. 25–37.